RÉPUBLIQUE FRANÇAISE
Liberté
Égalité
Fraternité

ENAC

End of Study Memory

Last update: October 22, 2025

Integration of R-Mode MSK Broadcasts and PVT Solutions for Stable Clock Synchronization in the Baltic Sea

Presented on November, 2025 by

BEN LARBI Malek

Promotion:

ASNAT23

Supervised at **Deutsches Zentrum für Luft- und Raumfahrt (DLR)** by

GRUNDHÖFER Lars

Acknowledgement

I would like to express my deepest gratitude to my former professors at the **École Nationale de l'Aviation Civile (ENAC)**, Toulouse, whose exceptional teaching and guidance laid the foundation for my understanding of navigation and communication engineering. The quality and rigor of their courses were instrumental in enabling me to feel confident and at ease throughout this internship.

My sincere thanks also go to **Daniel Medina** and **Andrea Bellés Ferreres**, who formed the interview team at DLR and opened the door for this new adventure. Their trust and support have meant a great deal to me. I am truly grateful that they believed in my potential, conducted my interview with kindness and professionalism, and helped place me in the department best suited to my interests.

I am especially grateful to my supervisor at **DLR**, **Lars Grundhöfer**, for his careful guidance and attentive supervision. His patience and insightful feedback greatly enhanced my learning experience. I am also deeply thankful to **Stefan Gewies**, the group leader, whose clarity, direction, and continuous support were crucial in guiding me along the right path. I would further like to thank the rest of the brilliant research team, who, despite being somewhat distant from my topic, were always insightful, willing to help, and eager to share their expertise.

To all of you: thank you for making this journey both enriching and inspiring.

Abstract

Time synchronization plays a critical role in modern maritime navigation, enabling precise positioning, coordination, and safety. While Global Navigation Satellite Systems (GNSS) remain the foundation for positioning and timing, vulnerabilities such as jamming and spoofing,especially in the Baltic Sea, have driven the development of complementary systems such as R-Mode.

This thesis investigates time extraction methods from Minimum Shift Keying (MSK) signals within the R-Mode system, evaluates synchronization accuracy, and explores techniques for stabilizing a local clock oscillator against remote atomic clock references to obtain a stable, up-to-date clock. The work combines theoretical analysis, GNU Radio implementation, and simulation to demonstrate the feasibility of resilient, synchronized maritime navigation beyond sole GNSS dependence.

Contents

List of Figures

List of Tables

List of Abbreviations

AIS	Automatic Identification System
CW	Continuous Wave
DGNSS	Differential Global Navigation Satellite System
DLR	German Aerospace Center (Deutsches Zentrum für Luft- und Raumfahrt)
DSC	Digital Selective Calling
ECDIS	Electronic Chart Display and Information System
FFT	Fast Fourier Transform
GNSS	Global Navigation Satellite System
GPS	Global Positioning System
IALA	International Association of Marine Aids to Navigation and Lighthouse Authorities
Inmarsat	International Maritime Satellite Organization
LORAN	Long Range Navigation
MSK	Minimum Shift Keying
OCXO	Oven-Controlled Crystal Oscillator
PVT	Position, Velocity, Time
RTCM	Radio Technical Commission for Maritime Services
RTOS	Real-Time Operating System
Rx	Receiver
SDR	Software-Defined Radio
SPS	Standard Positioning Service
SZC	Standard Zero Crossing
TCXO	Temperature-Compensated Crystal Oscillator
Tx	Transmitter
UTC	Coordinated Universal Time
VDR	Voyage Data Recorder
VHF	Very High Frequency

List of Symbols and Constants

Symbol	Description	Value / Unit / Formula
c	Speed of light in vacuum	2.9979×10^8 m/s
f_c	Carrier frequency (general)	≈ 300 kHz
ω_c	Angular carrier frequency	$\omega_c = 2\pi f_c$ (rad/s)
f_1, f_2	CW1 and CW2 frequencies	e.g. 307,775 Hz, 308,225 Hz
ω_1, ω_2	Angular frequencies of CW1, CW2	$\omega_i = 2\pi f_i$ (rad/s)
A_1, A_2	Amplitudes of CW1 and CW2	(signal amplitude units)
ϕ_1, ϕ_2	Phase of CW1 and CW2 at receiver (propagation)	rad
$\varphi, \varphi_{\text{beat}}$	Generic phase; beat phase (CW1+CW2)	rad
λ_1, λ_2	Wavelengths of CW1, CW2	$\lambda_i = c/f_i$ (m)
λ_{beat}	Beat wavelength	$\lambda_{\text{beat}} = \dfrac{\lambda_1 \lambda_2}{\lvert\lambda_1 - \lambda_2\rvert}$
D	Geometric Tx–Rx distance	m
τ	Delay (context dependent)	s
T_{bit}	Bit duration	$1/R_b$ (s)
R_b	Bit rate	100 bps
T_{obs}	Observation time	s
F_s	Sampling frequency	Hz
N	Number of samples	$N = T_{\text{obs}} F_s$
b	Bandwidth / half-sample term	e.g. $b = F_s/2$
SNR	Signal-to-noise ratio	dB
σ^2	Noise variance	—
N_0	Noise spectral density	W/Hz
$J(\theta)$	Fisher Information Matrix	—

Chapter 1

Introduction

The modern world is increasingly dependent on precise positioning, navigation, and timing (PNT) technologies, which together form the backbone of global transportation, communication, and information systems. From the synchronization of telecommunication networks and power grids to the safe operation of maritime and aviation systems, accurate timekeeping and resilient navigation capabilities are indispensable to the functioning of modern societies. However, the growing reliance on Global Navigation Satellite Systems (GNSS) has also revealed the inherent vulnerabilities of space-based infrastructures, particularly in regions where jamming, interference, or intentional spoofing can severely disrupt operations. These vulnerabilities underscore the urgent need for complementary terrestrial systems capable of ensuring continuity of service under degraded or denied GNSS conditions.

In this context, research into alternative and hybrid PNT solutions has become a central focus within the scientific and engineering communities. Among these, the development of terrestrial backup systems such as Enhanced LORAN (eLORAN) and Ranging Mode (R-Mode) technologies offers a promising approach to strengthening the resilience of navigation and timing infrastructures. Such systems exploit existing maritime broadcast networks to deliver reliable, ground-based signals that can be used for both position determination and time synchronization. Their integration with advanced signal processing and software-defined radio (SDR) techniques provides a path toward achieving autonomous and robust synchronization capabilities, even in challenging radio-frequency environments.

This thesis is situated within this evolving landscape of resilient navigation research. It addresses one of the key challenges in the realization of R-Mode systems, accurate time extraction and clock stabilization based on Minimum Shift Keying (MSK) signals transmitted by maritime beacons in the Baltic Sea. By focusing on the intersection of communication theory, signal processing, and synchronization engineering, this work contributes to the broader objective of developing dependable timing architectures for future maritime navigation networks. Through theoretical analysis, numerical simulation, and experimental validation, the study aims to demonstrate how precise time recovery from terrestrial signals can serve as a cornerstone for GNSS-independent navigation and timing systems, thereby reinforcing the integrity and resilience of global maritime operations.

1.1 The German Aerospace Center (DLR)

The Deutsches Zentrum für Luft- und Raumfahrt (DLR) is the Federal Republic of Germany's national research institution for aeronautics, space, energy, transportation and digitalisation. It

traces its lineage to early-20th-century institutes such as the Aerodynamische Versuchsanstalt (founded in 1907) and the Deutsche Versuchsanstalt für Luftfahrt (formed in 1912). In 1969, those and other institutes were merged to form the Deutsche Forschungs- und Versuchsanstalt für Luft- und Raumfahrt (DFVLR). In 1989 the DFVLR was renamed Deutsche Forschungsanstalt für Luft- und Raumfahrt (DLR). Finally, on 1 October 1997 the DLR merged with the Deutsche Agentur für Raumfahrtangelegenheiten (DARA) and assumed the current name, Deutsches Zentrum für Luft- und Raumfahrt (DLR). From that point onwards, DLR expanded its remit into multidisciplinary research, combining fundamental research and applied technology development, and addressing scientific, technological and societal challenges in aviation, spaceflight, sustainable energy systems, transportation technologies and advanced communication infrastructures.[6]

Its work combines scientific inquiry with engineering innovation, and supports both the German federal government (including management of national space programmes) and international space missions, in collaboration with organisations such as the European Space Agency (ESA), NASA, and numerous industrial and academic partners. DLR's research ecosystem spans more than 55 institutes and facilities, distributed across multiple locations in Germany (including Cologne, Oberpfaffenhofen, Bremen, Braunschweig, Berlin-Adlershofen and Neustrelitz). These sites host interdisciplinary teams of engineers, physicists, mathematicians and computer scientists who contribute to a broad range of projects, from developing next-generation satellites and spacecraft to advancing quantum communication and renewable energy systems.[6]

The organisation maintains its own laboratories, flight-test platforms and simulation environments, enabling it to prototype and evaluate technologies under realistic operational conditions. This integrated approach ensures that research outcomes are not only scientifically sound but also directly applicable to industrial and governmental needs.[7].

Figure 1.1: DLR Locations across Germany, marked by red dots

The organization maintains its own laboratories, flight test platforms, and simulation environments, allowing it to prototype and evaluate technologies under realistic operational conditions. This approach ensures that research outcomes are not only scientifically sound but also directly applicable to industrial and governmental needs.

1.1.1 Institute of Communications and Navigation (KN)

Within DLR, the Institute of Communications and Navigation (Institut für Kommunikation und Navigation, KN) is one of the leading centers dedicated to the advancement of technologies for reliable information transfer, precise positioning, and synchronization in both terrestrial and space environments. KN's mission is to develop and demonstrate innovative communication and navigation systems that enable robust connectivity, high data rates, low latency, and secure information exchange. These systems are crucial to the success of modern aerospace missions, as well as emerging applications such as autonomous vehicles, quantum networks, and Earth observation constellations. [8] KN operates several experimental facilities, such as the Optical Ground Station Oberpfaffenhofen [9], the GNSS Test and Innovation Facility (GATE) [10], and

specialized laboratories for frequency reference systems and synchronization experiments. These facilities enable the institute to perform end-to-end system testing from algorithm development to hardware validation.

1.2 Research Context and Ongoing Projects

The rapid evolution of communication and navigation technologies has intensified the demand for ultra-stable frequency generation and precise synchronization. Several ongoing projects within DLR address these challenges.

1.2.1 Motivation for the Internship Project

The internship project titled "Integration of R-Mode MSK Broadcasts and PVT Solutions for Stable Clock Synchronization in the Baltic Sea" was initiated within DLR's Communication Systems Division as part of an ongoing effort to enhance the frequency reference reliability and synchronization performance of high-precision navigation and communication payloads. The ability to generate, acquire, and maintain phase-coherent local oscillators is of fundamental importance for a wide range of DLR projects from satellite-based navigation to R-Mode terrestrial backup systems and time dissemination networks. The specific motivation for this internship emerged from the increasing need for robust synchronization architectures capable of operating autonomously and continuously, even under adverse environmental or signal conditions (i.e interference or jamming). In particular, the R-Mode (Ranging Mode) system (a terrestrial navigation technology designed to complement and back up Global Navigation Satellite Systems (GNSS)) requires highly stable local oscillators whose frequencies can be precisely aligned with signals received from remote transmitters.

This thesis focuses on the design, implementation, and evaluation of timing extraction techniques within the R-Mode framework. Specifically, the research investigates methods for obtaining high-accuracy time information from MSK-modulated R-Mode signals and for stabilizing a local oscillator using feedback control loops. These techniques aim to maintain synchronization over extended periods, even in the absence of GNSS signals.

The overarching objective is to develop a robust timing subsystem capable of supporting resilient maritime navigation and critical timing services. Through theoretical modeling, simulation, and experimental validation, this research seeks to contribute to the realization of an operational R-Mode network as part of the broader strategy for GNSS backup and augmentation in the maritime domain.

To achieve such synchronization, DLR required a flexible Software-Defined Radio (SDR) platform capable of receiving MSK (Minimum Shift Keying) modulated data streams transmitted by remote R-Mode stations, extracting precise time information, and using this information to control and stabilize a local oscillator through a closed-loop feedback system. The broader motivations for this work can be summarized as follows:

Stringent performance requirements: Accurate timing and frequency stability are critical for ranging accuracy in R-Mode systems. Phase fluctuations or clock drift in the local oscillator can directly degrade the positioning accuracy and introduce timing offsets in the decoded data stream, certificates authentication and validation, as well as other maritime operations mentioned in section 1.4

Advancement of SDR-based synchronization: Software-Defined Radio platforms provide a versatile environment for implementing advanced digital signal processing algorithms for synchronization and stabilization. By leveraging SDR technology, DLR can rapidly prototype and validate new synchronization architectures before deploying them in hardware.

Resilience and redundancy in navigation systems: The R-Mode concept aims to provide a GNSS-independent backup for positioning, navigation, and timing (PNT) services. This requires highly reliable ground-based receivers that can maintain synchronization autonomously, even during temporary loss of GNSS coverage or interference.

Support for future DLR projects: The results of this internship directly contribute to DLR's R-Mode testbed activities and to broader research efforts on hybrid navigation and time transfer systems. The developed SDR system forms a building block for future experimental setups (and frequency stability studies at DLR's Institute of Communications and Navigation.

1.3 Navigation and Timekeeping

The disciplines of navigation and timekeeping have been intertwined throughout the evolution of human exploration and maritime science. The ability to determine one's position on Earth, especially at sea, has always depended on the precise measurement of time. During the Age of Discovery, navigators could estimate latitude using celestial observations, but longitude determination remained an elusive problem for centuries. Errors in longitude estimation could result in catastrophic navigational mistakes, leading to shipwrecks, lost cargo, and loss of life.

The eighteenth century marked a turning point when the British government offered the Longitude Prize to anyone who could develop a practical method for determining longitude at sea with sufficient accuracy. This challenge inspired John Harrison, a self-taught clockmaker, to design a series of marine chronometers capable of maintaining time at sea despite the effects of temperature fluctuations, humidity, and ship motion. His invention enabled navigators to compare local time (determined by the Sun) with Greenwich Mean Time (kept by the chronometer), thereby calculating longitude precisely. Harrison's chronometers effectively revolutionized global navigation, marking the beginning of precise timekeeping as a cornerstone of navigation. [11]

1.4 From Chronometers to Atomic Clocks

In the modern era, navigation has transitioned from mechanical chronometers to satellite-based systems that depend on the unparalleled accuracy of atomic clocks. The advent of Global Navigation Satellite Systems (GNSS), including the American GPS, European Galileo, Chinese BeiDou, and Russian GLONASS, has transformed global navigation, enabling real-time positioning, navigation, and timing (PNT) on a global scale. These systems function by measuring the travel time of radio signals transmitted by satellites orbiting the Earth. Each satellite carries multiple synchronized atomic clocks, broadcasting precise time references and orbital data.

A GNSS receiver determines its position by calculating the difference between the transmission and reception times of signals from at least four satellites. This time difference is converted into a distance (or range), allowing the receiver to triangulate its position. However, this process is extraordinarily sensitive to timing accuracy: a clock error of just one nanosecond corresponds to a positional error of approximately 30 centimeters. Even a small offset in the receiver's internal

clock,if not properly synchronized,can lead to cumulative errors of tens of meters. For maritime vessels navigating in congested ports, narrow straits, or shallow waters, such discrepancies can pose significant safety risks.

1.5 Vulnerabilities of GNSS and the Need for Resilient Timing

Although GNSS provides unparalleled precision and global coverage, its signals are inherently weak by the time they reach Earth's surface, typically around -130 dBm. As a result, they are highly susceptible to interference, jamming, and spoofing. Unintentional interference can originate from malfunctioning equipment or overlapping frequency bands, while intentional interference (jamming) or deceptive signal generation (spoofing) can cause false positioning information or total loss of service.

Given the maritime sector's dependence on GNSS for navigation, communication, and operational timing, such vulnerabilities represent a major threat to critical infrastructures. A GNSS outage could disrupt not only ship navigation but also port operations, air traffic management, financial networks, and power distribution systems that depend on precise timing synchronization[12]. This has prompted the search for terrestrial backup systems capable of maintaining positioning and timing continuity when GNSS is degraded or denied.

1.6 Time as the foundation of Maritime Operations

1.6.1 Communication and Coordination

Maritime communication systems rely extensively on synchronized timing to ensure data integrity and operational efficiency. Cargo ships continuously exchange data with ports, coastal authorities, and other vessels through a combination of radio and satellite communication channels. Systems such as Digital Selective Calling (DSC), Inmarsat, and Very High Frequency (VHF) radio depend on precisely synchronized clocks to ensure that data packets are transmitted and received in the correct order.

Similarly, the Automatic Identification System (AIS), a mandatory system for most commercial vessels, broadcasts information such as the ship's position, course, speed, and identification number at defined intervals. These transmissions are synchronized to a global time reference to prevent signal overlap and ensure that each vessel's data can be correctly interpreted by others. Inconsistent or unsynchronized timing could result in overlapping signals, data corruption, or misinterpretation of vessel movements, jeopardizing navigational safety.

1.6.2 Safety and Incident Investigation

Accurate and synchronized timekeeping also plays a crucial role in maritime safety management and accident investigation. The Voyage Data Recorder (VDR), often referred to as the maritime "black box", continuously records navigational data, bridge audio, radar imagery, and communication logs. In the aftermath of an incident such as a collision, grounding, or act of piracy, investigators depend on precise timestamps to reconstruct the sequence of events.

When the timestamps of the VDR, radar, Electronic Chart Display and Information System (ECDIS), and engine monitoring systems are synchronized, it becomes possible to establish cause-and-effect relationships between different events. For example, investigators can determine

whether a ship's change in course occurred before or after a radio communication, or whether an engine failure coincided with a navigational command. Without synchronized timing, such analysis would be unreliable, hindering both safety improvements and legal accountability. [13]

1.6.3 Legal and Commercial Considerations

Timekeeping also has direct implications for maritime commerce and law. International shipping operations involve complex logistical chains and legal frameworks that depend on precise temporal documentation. Bills of lading, cargo manifests, and customs declarations require accurate timestamps to verify compliance with contractual and regulatory requirements. In disputes over insurance claims or contractual obligations, the ability to demonstrate when a ship entered a specific maritime zone or when cargo was loaded or unloaded is often decisive. Thus, the reliability of timekeeping extends beyond navigation and safety,it underpins the legal and financial trust that sustains global maritime trade.

1.6.4 Engineering and Operational Efficiency

From an engineering perspective, synchronized timekeeping enhances vessel performance monitoring and fleet management. Shipboard systems continuously log data from engines, generators, propulsion units, and environmental sensors. Accurate timestamps enable meaningful correlation between these datasets, allowing engineers to analyze trends, diagnose anomalies, and optimize operations.

For fleet operators managing multiple vessels, synchronized clocks allow comparative performance analysis and coordinated fleet operations. Data such as fuel consumption, engine load, and voyage duration can be aligned temporally to identify inefficiencies and optimize routing strategies. In this context, time synchronization is a cornerstone of digital maritime transformation, supporting predictive maintenance, remote diagnostics, and integration with shore-based analytics platforms.

Chapter 2

State of the Art of ground-based navigation and time service

2.1 Enhanced LongRAngeNavigation (eLORAN)

Enhanced Loran is a terrestrial radio navigation system developed as a resilient complement to Global Navigation Satellite Systems. Unlike GNSS, which relies on weak space-based signals, eLoran operates in the Low Frequency band (90–110 kHz) and transmits high-power ground-wave signals from terrestrial stations. This allows for reliable coverage over long distances and high resistance to interference, jamming, or signal blockage.

Each eLoran station emits a sequence of precisely timed pulses organized into chains with unique Group Repetition Intervals, enabling receivers to identify transmitting stations. High-power transmission, typically in the hundreds of kilo Watts to mega Watts range, ensures wide-area coverage and strong signal reception even in urban or obstructed environments.

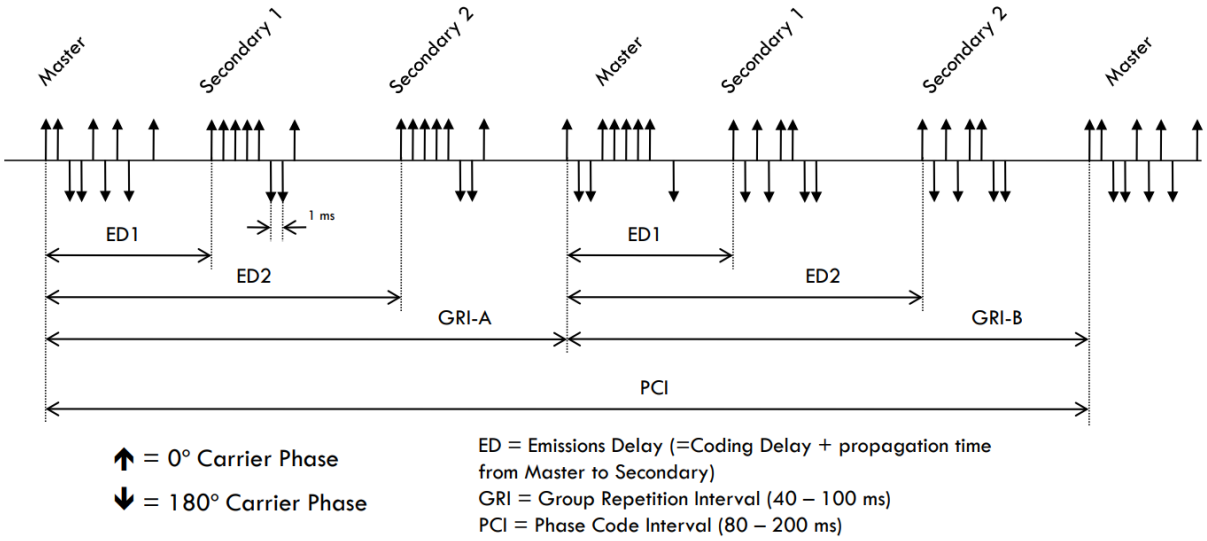

Figure 2.1: Train of signals emitted by eLORAN [1]

This architecture was kept for legacy purposes (In loran-C Master pluses slaves emit at reception

of pulse, eLORAN: stations emit according to a predefined schedule based on UTC but gives off virtually the same result only more stable and not prone to environment)[1]

$$r_{\text{master}} = \sqrt{(x - x_i)^2 + (y - y_i)^2} = c\left(t_{\text{master\_reception}} - t_{\text{master\_transmission}}\right) \tag{2.1}$$

$$r_n = \sqrt{(x - x_j)^2 + (y - y_j)^2} = c\left(t_{\text{n\_reception}} - t_{\text{n\_transmission}}\right) \tag{2.2}$$

$$= c\left(t_{\text{n\_reception}} - \left(t_{\text{master\_transmission}} + \text{known delay}(n)\right)\right) \tag{2.3}$$

where $t_{\text{master\_reception}}$ is the time of reception of the Master station's signal, $t_{\text{n\_transmission}}$ is the time of emission of the Master station's signal, $t_{\text{n\_reception}}$ Positioning is based on measuring the Time of Arrival (ToA, also the base of circular position) of signals from multiple stations. By intersecting the resulting circles of potential positions, a receiver can calculate its location.

Known delay is the time it takes for the master pulse to trigger the slave emission.

eLoran is backward compatible with LORAN-C and enables positioning based on measuring the Time Difference of Arrival (TDoA) between signals from multiple stations. By intersecting the resulting hyperbolas of position, a receiver can calculate its location.

Since the position is unknown so is the time of transmission, but we access to the time of reception of each station's signal (timestamp that the receiver locally provides).

$$\begin{aligned} r_i - r_j &= c\left(t_i - t_j + \text{delay}(i) - \text{delay}(j)\right) \\ &= \sqrt{(x - x_i)^2 + (y - y_i)^2} - \sqrt{(x - x_j)^2 + (y - y_j)^2} \end{aligned} \tag{2.4}$$

$$\begin{aligned} r_i - r_k &= c\left(t_i - t_k + \text{delay}(i) - \text{delay}(k)\right) \\ &= \sqrt{(x - x_i)^2 + (y - y_i)^2} - \sqrt{(x - x_k)^2 + (y - y_k)^2} \end{aligned} \tag{2.5}$$

The transmission time being eliminated by computing the difference, we now have two equations The two unknowns x and y. The remaining step is to detect the time of arrival

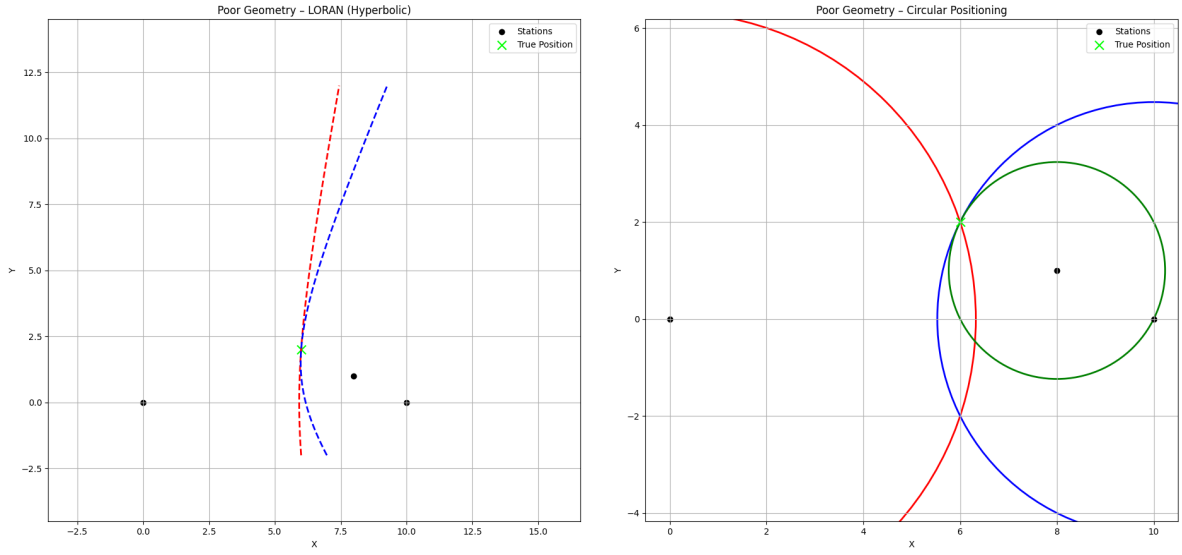

Figure 2.2: LORAN poor geometry comparison: Circular intersection right and hyperbolic intersections left

The stations are usually situated on the coasts; therefore, they are almost aligned, offering bad geometry. For the same position, the circular intersections have a greater angle offering better precision, whereas the hyperbolas intersect at quasi null angles, making the uncertainty about the position greater

The standard eLoran pulse is defined as i(t),

$$i(t) = \begin{cases} A(t-\tau)^2 \exp\left[\dfrac{-2(t-\tau)}{65}\right] \sin(0.2\pi t + PC), & \tau \leq t \leq 65+\tau, \\ 0, & t \leq \tau \end{cases} \tag{2.6}$$

where: A is the normalization constant related to the magnitude of the peak antenna current in amperes. t is the time measured in microseconds. τ is the envelope-to-cycle discrepancy measured in seconds and PC is the phase code. The above equation produces the following pulse shape.

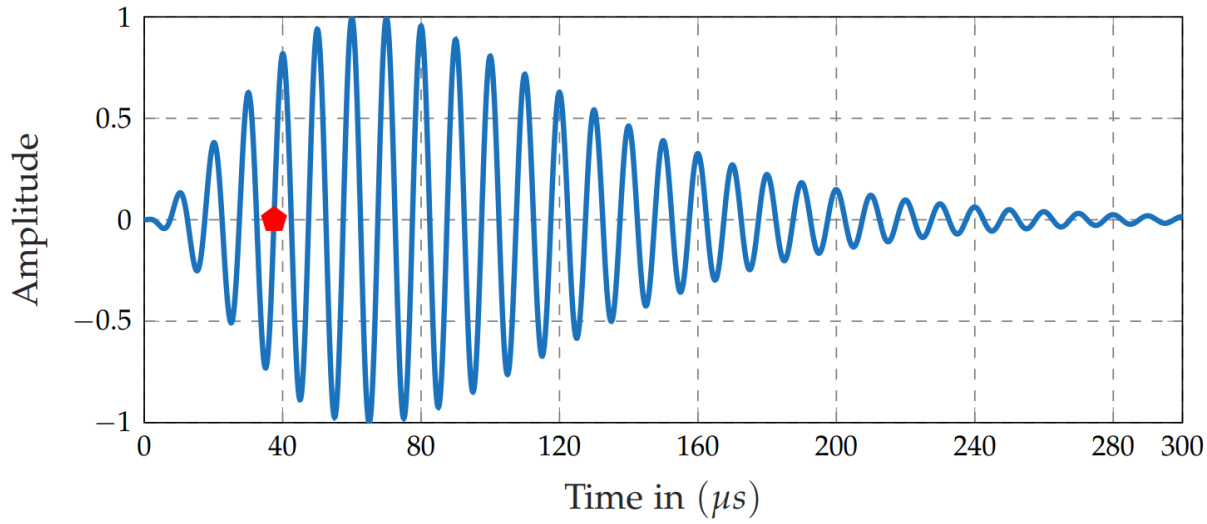

Figure 2.3: The standard eLORAN pulse a tear drop shape, the SZC (defined as the 6th zero crossing) has been indicated with a red dot [2]

The pulse is shaped and optimized in a way that reduces skywave interference and facilitates the estimation of ToA

The method of estimating the time of arrival revolves around SZC detection. However, for a fair comparison with the R-Mode tentative ToA estimation using the MSK we shall work with the matched filter method, although the same is true for the SZC detection method.

To assess the effectiveness of the correlation-based Time of Arrival estimation under different noise environments, a Monte Carlo simulation is conducted. In this simulation, Gaussian noise with varying power levels is added to the received eLORAN signal. For each noise level, multiple realizations of the noisy signal are generated, and the correlation output is computed to estimate the ToA. The resulting estimates are then statistically analyzed, and the standard deviation of the estimated ToA values is plotted as a function of the noise power (or SNR). This approach provides insight into the performance and noise sensitivity of the correlation-based estimator.

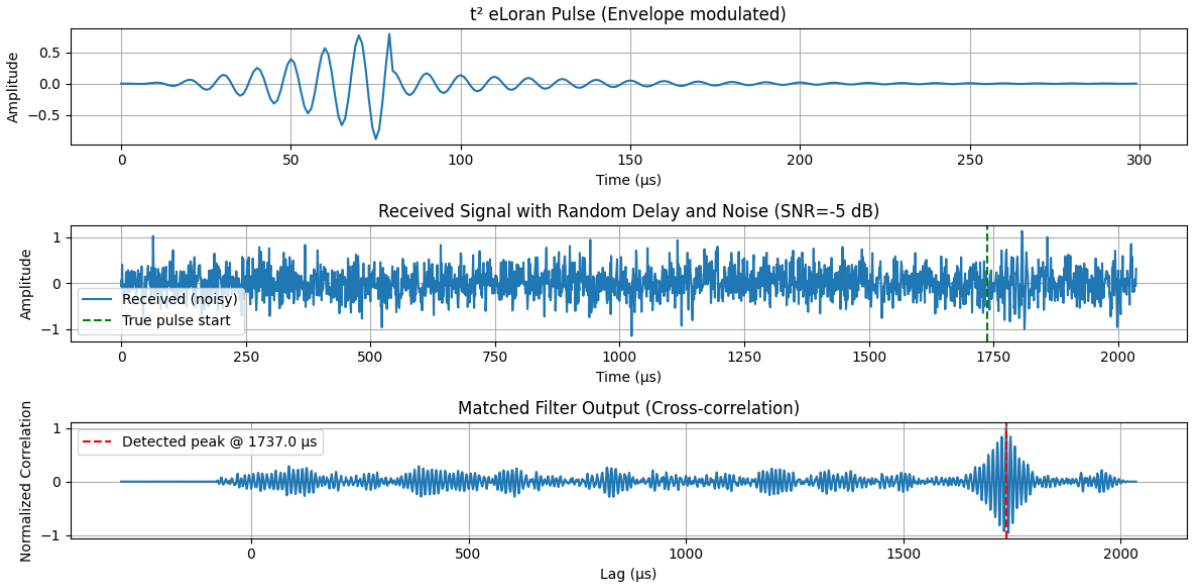

Figure 2.4: Estimating TOA of loran pulse through matched filter + peak detection

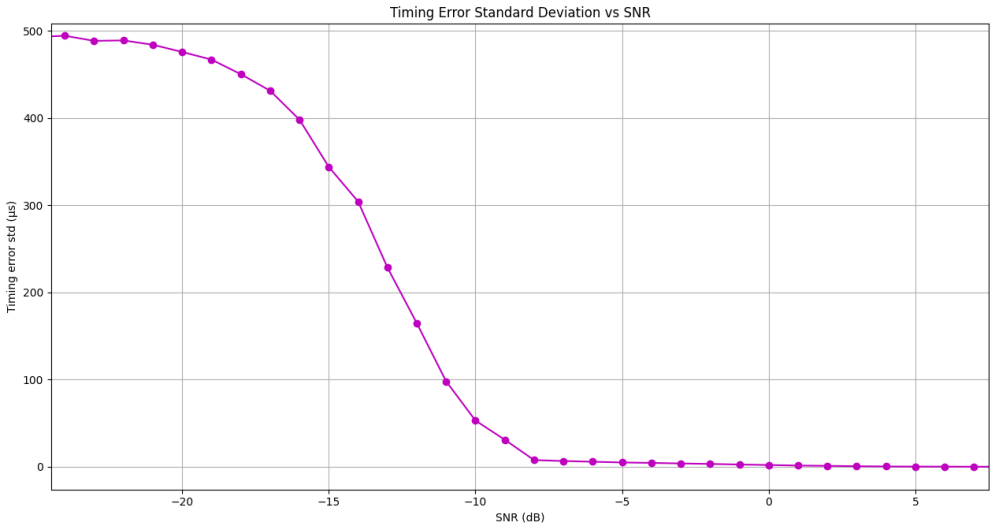

Figure 2.5: Montecarlo simulation results, timing standard deviation vs SNR

The higher the SNR, the more accurate is the estimate of the TOA (SNR being defined at the input of the receiver)

The timing error virtually reaches 0 at an SNR of 6dB

In addition to navigation, eLORAN provides precise timing, synchronized to Coordinated Universal Time (UTC) using atomic clocks. Receivers can extract Stratum-1 quality timing (<50 ns accuracy with differential corrections) [14]

which is critical for telecommunications, power grids, and financial systems. Embedded Low-Rate Data Channels (LDC) allow transmission of corrections, integrity messages, and system information directly to users, further enhancing accuracy and reliability.

The propagation of the system's ground-wave ensures robustness in environments where satellite signals may be unavailable or degraded. Typical coverage per station ranges from 1000 to 1500 km. eLORAN has been employed in maritime navigation, aviation, and as a resilient timing source for critical infrastructure, providing a terrestrial alternative to GNSS while maintaining both navigation and timing capabilities[14]

Chapter 3

The R-Mode System: A Resilient Terrestrial Alternative

3.1 R-Mode presentation

In response to growing concerns about GNSS vulnerability, and due to the absence of eLORAN broadcasting stations in the region of interest, researchers have explored R-Mode (Ranging Mode) as a promising terrestrial backup system. R-Mode leverages existing medium-frequency (MF) maritime radio infrastructure, traditionally used for communication and navigation, to deliver resilient positioning and timing information without relying on satellites. The system transmits Minimum Shift Keying (MSK)-modulated signals that can be received by standard maritime equipment. By analyzing the phase and timing of these signals, receivers can derive both range and precise time references.

The principal advantage of R-Mode lies in its ability to repurpose existing coastal radio networks, minimizing infrastructure costs while extending coverage to critical maritime zones such as ports, harbors, and coastal approaches. This terrestrial approach offers robustness against GNSS disruptions and provides a foundation for a hybrid PNT architecture, where satellite and terrestrial systems complement each other to enhance reliability and resilience.

The DGNSS stations (prior to their conversion to R-Mode, presented on the map below) function as a means of transmitting DGNSS correction messages following the RTCM standard.

The International Telecommunication Union (ITU) specifies the use of marine DGNSS radio beacons in Recommendation M.823-2.

According to the latter standard, GNSS code-differential corrections are broadcast as a Minimum Shift Keying (MSK) signal, with carrier frequencies ranging from 283.5 kHz to 315 kHz in Europe (500 Hz bandwidth) and from 285 kHz to 325 kHz in North America (1000 Hz bandwidth). Operators may select bit rates of 50, 100, or 200 bits/s. In this study, we focus on 100 bits/s rate, as currently deployed in the Baltic Sea testbed.

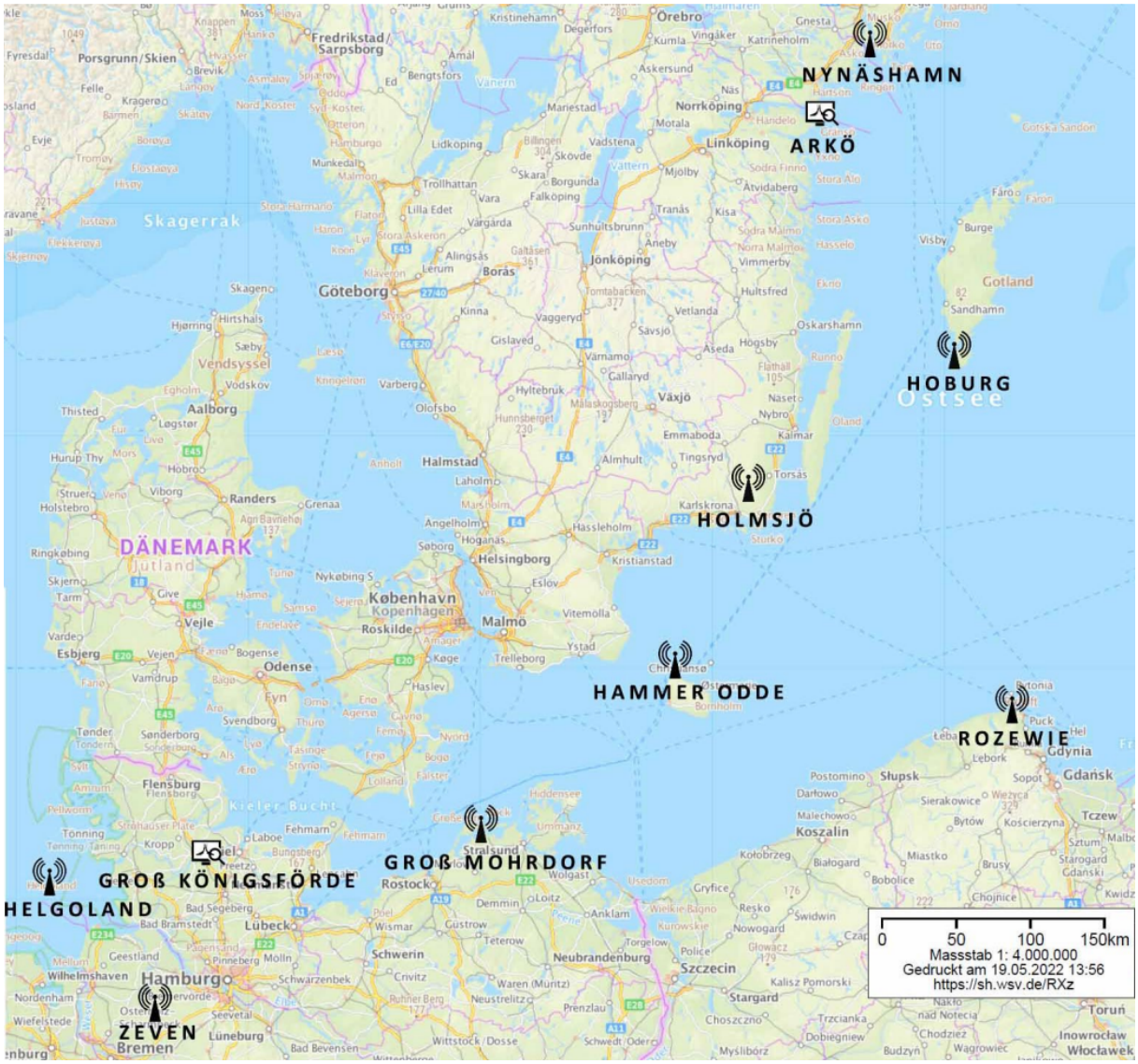

Figure 3.1: MF R-Mode testbed [3]

The spatial configuration of the antennas, as represented on the map, exhibits a favorable geometric distribution for earth's surface positioning applications. Their relative placement ensures good geometric dilution of precision (low HDOP) characteristics, minimizing position uncertainty and enhancing the accuracy and stability of the computed locations. This is one of the many factors that have pushed the development of R-Mode.

The MSK signal, centered at the carrier frequency f_c with amplitude A_{msk}, forms the core of the R-Mode transmission. For a single bit duration, it can be expressed as:

$$s_{\mathrm{MSK}}(t) = A_{\mathrm{MSK}} \sin\left(\omega_c t + b_\tau \frac{\pi t}{2T_{\mathrm{bit}}} + \varphi_{\mathrm{memory}}\right).$$

Here, b_τ represents the transmitted bit at time t, T_{bit} is the bit duration, ω_c is the angular carrier frequency, and $\varphi_{\mathrm{memory}}$ ensures phase continuity in MSK modulation.

Using the trigonometric formula $sin(at + b) = sin(at)cos(b) + cos(at)sin(b)$

$s_{msk}(t)$ can be rewritten as

$cos(2\pi ft)(b \times \pi \times \frac{R}{2} + \varphi_{\text{memory}}) + sin(2\pi ft) \times cos(b \times \pi \times \frac{R}{2} + \varphi_{\text{memory}})$

which can be interpreted as $I(t)cos(2\pi ft) + Q(t)sin(2\pi ft)$

This modulation, with a bitrate R_b of 100bps, is equivalent to using a half sine pulse lasting $T_c = .02s$

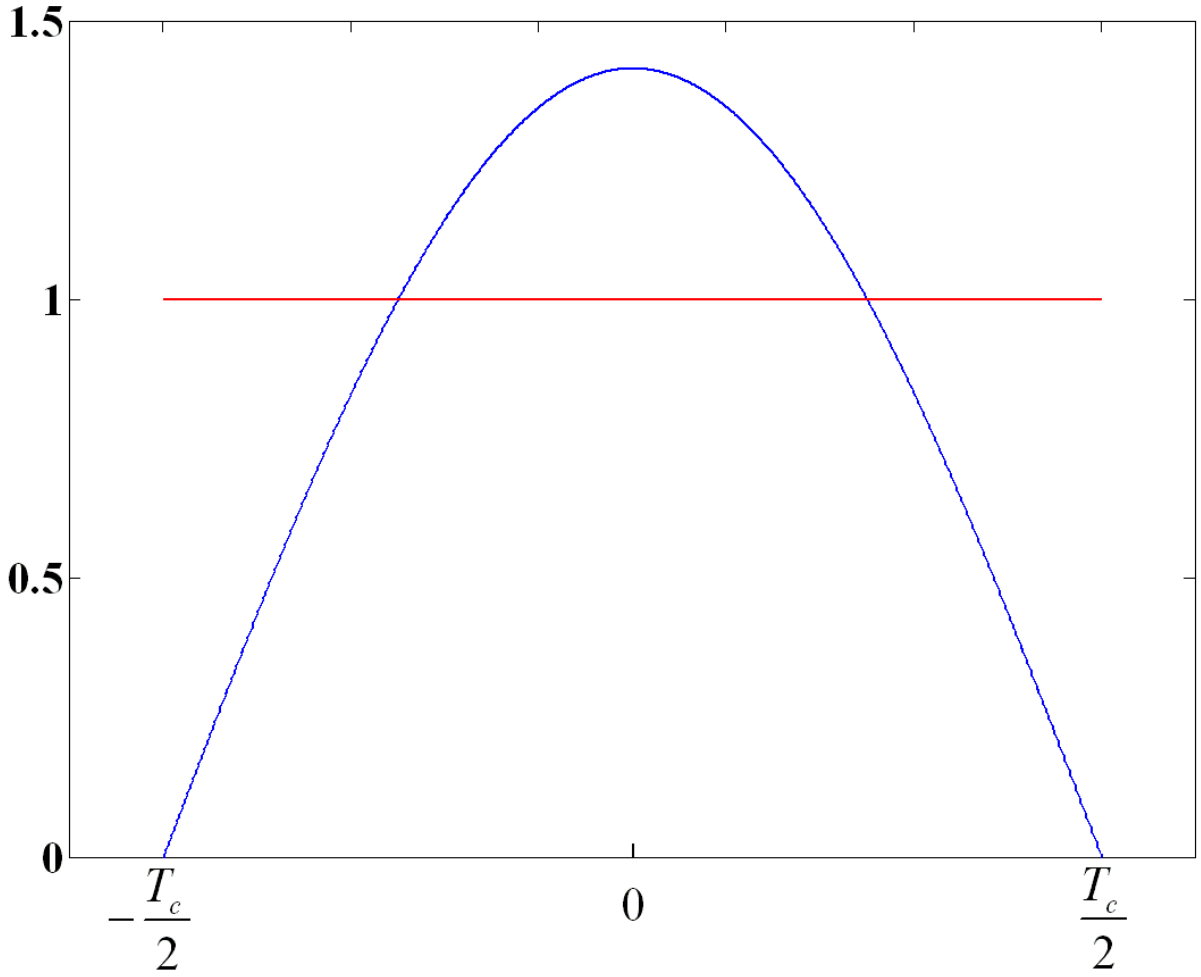

Figure 3.2: Half sine pulse shape of pulse $100 \times \frac{\pi}{4}$ and amplitude $\sqrt{2}$

The spectrum of this pulse wave is given by its fourier transform

$$S_{\text{MSK}}(\omega) = \int_{-T_{sc}/2}^{T_{sc}/2} \sqrt{2}\cos\left(\frac{\pi t}{T_{sc}}\right) e^{-j\omega t}\, dt = \sqrt{2}\int_{-T_{sc}/2}^{T_{sc}/2} \frac{e^{j\pi t/T_{sc}} + e^{-j\pi t/T_{sc}}}{2} e^{-j\omega t}\, dt \tag{3.1}$$

$$S_{\text{MSK}}(\omega) = j\sqrt{2}\cos\left(\frac{\omega T_{sc}}{2}\right)\left(\frac{1}{\frac{\pi}{T_{sc}} - \omega} + \frac{1}{\frac{\pi}{T_{sc}} + \omega}\right) = \frac{j\,2\sqrt{2}\pi\cos\left(\frac{\omega T_{sc}}{2}\right)}{T_{sc}\left(\frac{\pi^2}{T_{sc}^2} - \omega^2\right)} \tag{3.2}$$

So the normalized Power Spectral Density of the spreading MSK waveform is

$$G_{\text{MSK}}(\omega) = \frac{1}{T_{sc}}\left\|S_{\text{MSK}}(\omega)\right\|^2 = \frac{1}{T_{sc}}\frac{8\pi^2\cos^2\left(\frac{\omega T_{sc}}{2}\right)}{T_{sc}^2\left(\frac{\pi^2}{T_{sc}^2} - \omega^2\right)^2} \tag{3.3}$$

$$G_{\mathrm{MSK}}(f) = \frac{8 f_{sc}^3}{\pi^2} \frac{\cos^2\left(\frac{\pi f}{f_{sc}}\right)}{\left(f_{sc}^2 - 4f^2\right)^2} \tag{3.4}$$

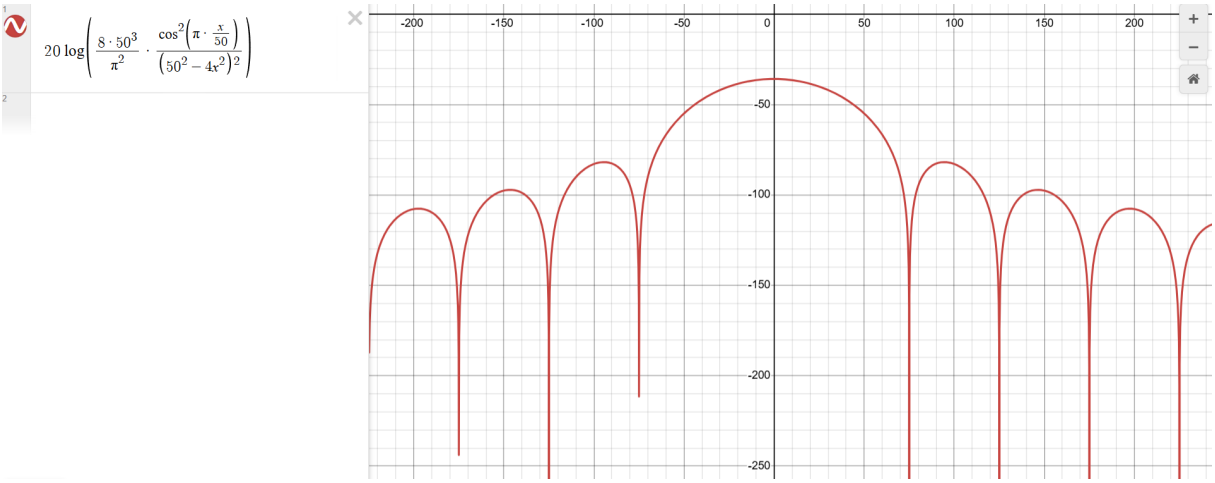

Figure 3.3: Plot of the MSK's PSD on a graphical calculator

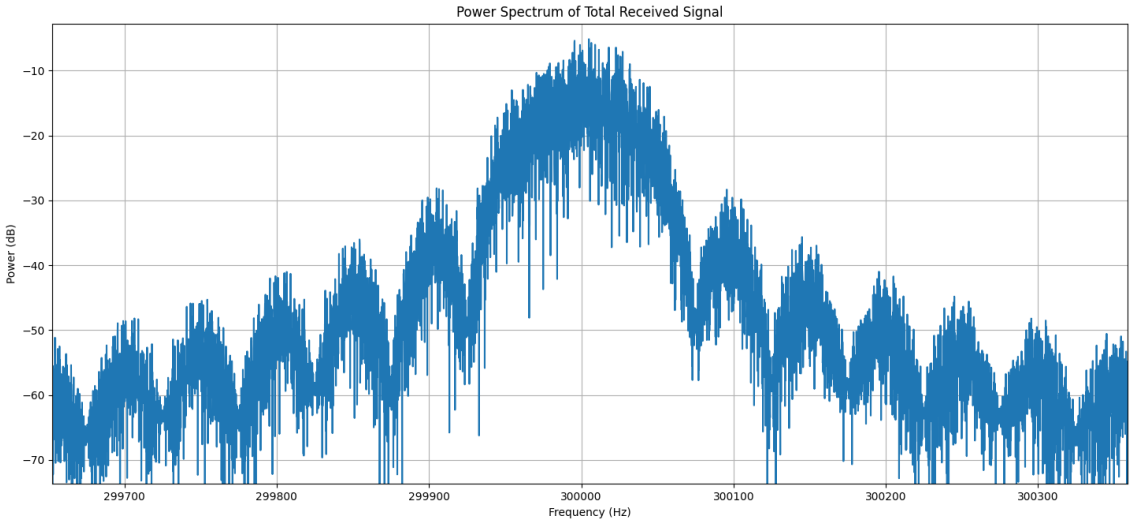

Figure 3.4: Python simulation of an MSK signal of central carrier 300khz (no noise)

Laying the theoretical and practical foundation about the spectrum of the legacy system on top of which we intend to improve is crucial for the future work.

3.2 New role : Autonomous navigation

This part of the study focuses on investigating the feasibility of using Differential GNSS broadcasting stations to enable autonomous navigation and precise time recovery. The key question

guiding this analysis is whether these existing infrastructures can be adapted or converted to support such functionalities without significant modification or additional deployment costs.

Before diving into the prospect of using the MSK signal for positioning, we first need to look at a similar system for analogy.

3.3 Feasibility of the Positioning using MSK

This idea operates on the same principle as LORAN (i.e determining distance from fixed stations), employing low-frequency ground-wave transmissions for precise and robust timing and positioning.

However, it differs in its station identification process and synchronization architecture. In traditional LORAN systems, station identification is implicitly encoded in the pulse sequence and timing structure, with a master–slave hierarchy that dictates transmission order, where the master station transmits first, followed by the slave stations after predetermined delays. The transmitted signals and their rate are different

In contrast, the system under study encodes station identifiers (IDs) directly within the Minimum Shift Keying (MSK) data message, thereby eliminating the need for a master–slave architecture. All transmitting stations are instead time-synchronized to a common reference and broadcast simultaneously, simplifying network coordination and improving scalability. Finally, compared to LORAN, the R-Mode stations do not transmit pulses.

To illustrate the signal processing procedure, we aim to determine the start of a data bit within the received MSK-modulated signal. This is achieved by performing a convolution (correlation) operation between the simulated received signal and a locally generated replica of the transmitted waveform. The resulting correlation output allows the identification of the bit start, which is in essence the ToA, which will in turn help estimate the range from one station. Doing so for multiple stations will enable trilateration.

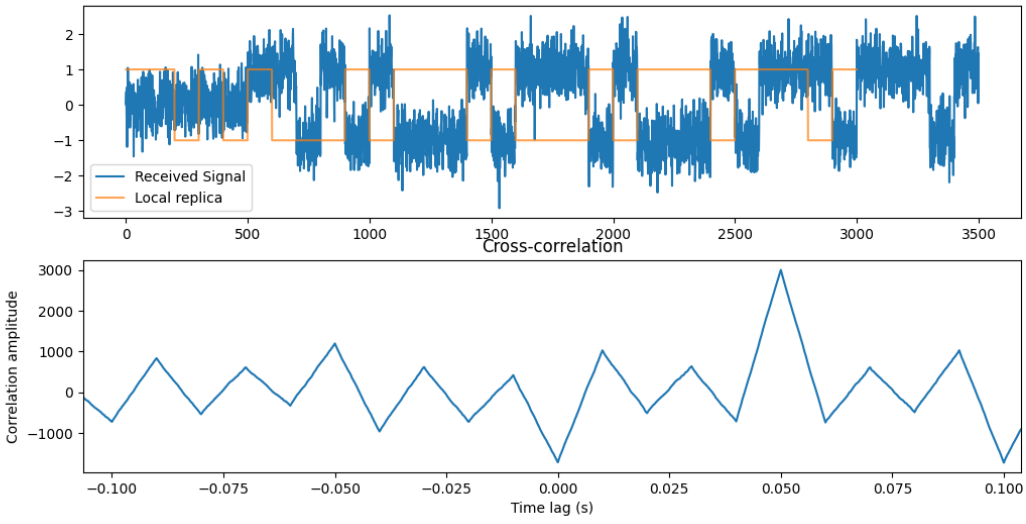

Figure 3.5: A simulation of a received square wave signal delayed by 50ms, correlated with a local replica to estimate the delay. (a peak at 50ms indicates a delay of 50ms)

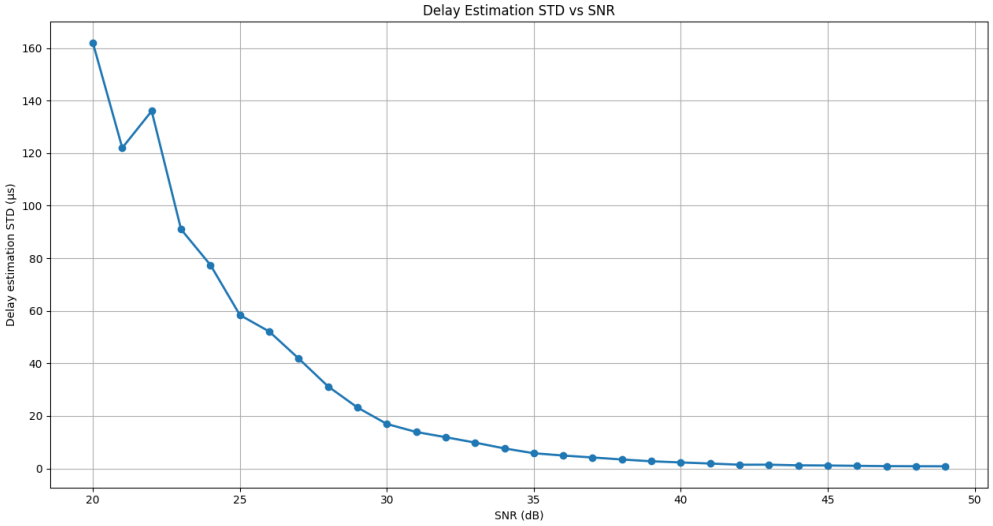

Figure 3.6: start delay estimation vs SNR Montecarlo simulation, bps=100, duration of 30bits

The delay standard deviation starts at a value 161.992µs corresponding to 20dB and drops to 1.148 µs corresponding to 45 dB SNR.

The key takeaway is the fact that due to the excessively low bitrate (100bps, hence the low number zero crossings in a certain period of time), estimating the TOA (Which is important for the hyperbolic or circular intersections described in 1.6.1) is an extremely difficult task, and since it is impossible to vary both the frequency of the already installed system(due to spectrum regulations / service specifications) or its power (due to current installation / Components limitations) the positioning task relying solely on MSK is to be abandoned.

Analytically the variance's analytical expression is [4]

$$\mathrm{var}(\hat{\tau}) = \sigma_{\hat{\tau}}^2 \geq \mathrm{MCRB}(\hat{\tau}) = \frac{2}{\pi^2 L_0 T\,\mathrm{SNR}} \tag{3.5}$$

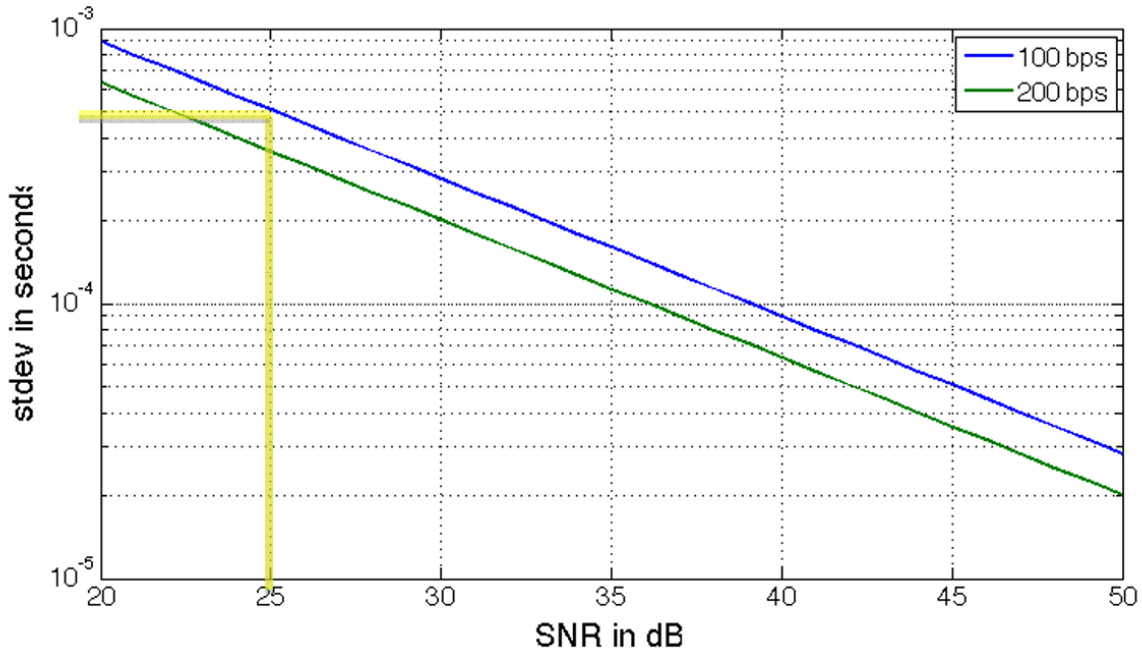

Figure 3.7: Plot of start delay from the modified CRB equation [4]

Referring to the above equation and plugging in the current system parameters of $L_0 = 30$, $T = .3$s SNR 25dB we obtain an error of around 33µs equivalent to 10km error.

3.3.0.1 Graphical interpretation of the effect of bitrate on time of arrival uncertainty

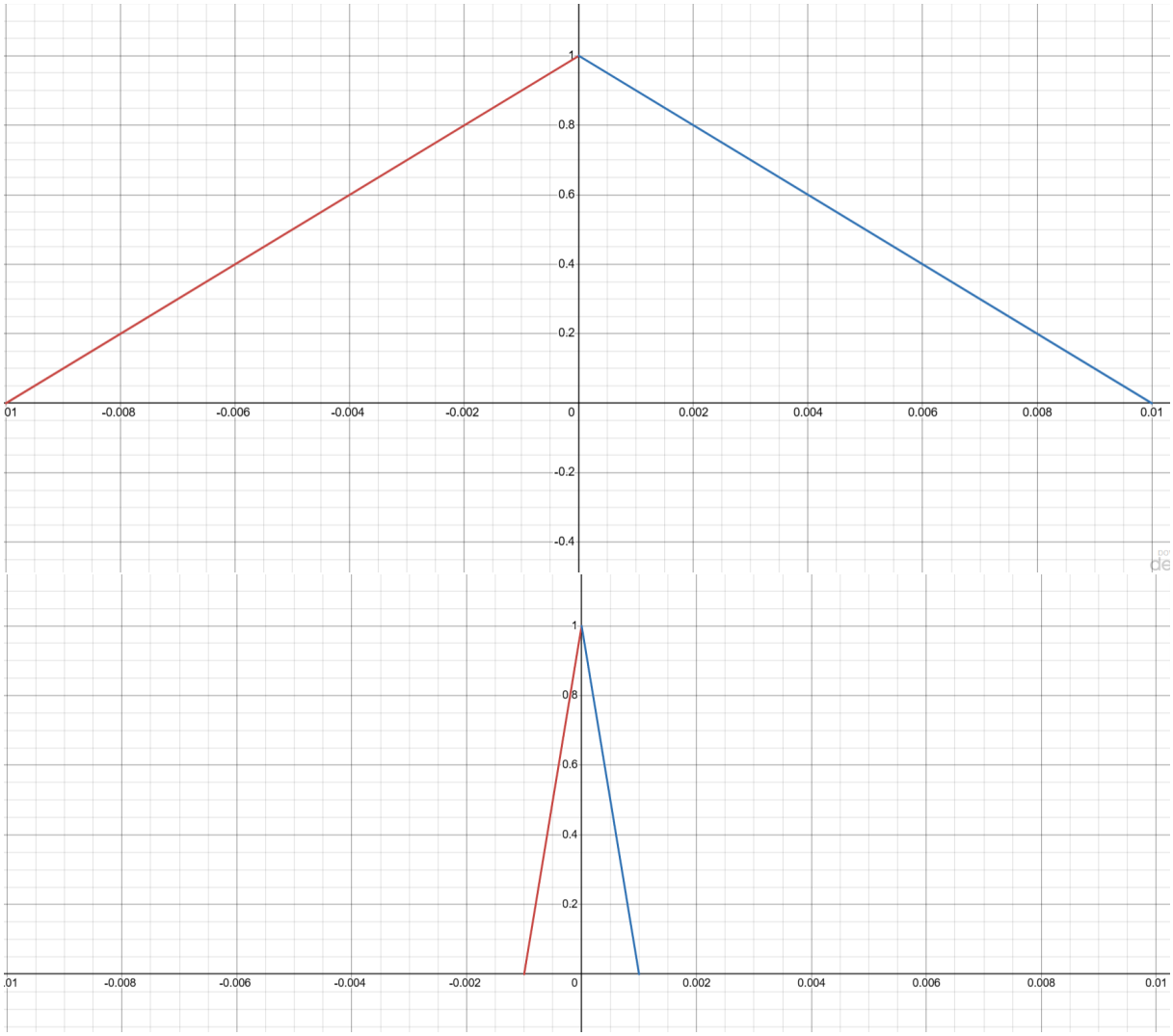

Figure 3.8: autocorrelation of a 100bps (top) and a 1kbps square signal (bottom)

For an equivalent amount of noise energy added to the matched filter output, the slower (100 bps) signal exhibits a broader temporal window in which noise can potentially elevate a value to become the new peak. In contrast, a rapidly decaying autocorrelation (1000 bps) constrains this window, reducing the likelihood that the same noise energy will make far surpass the true peak.

As a quantitative illustration based on the figure, if the noise energy is 0.2, the interval of delays where the noise could exceed the peak value of 1 is [-0.002, 0.002] for the slower signal, compared to [-0.0002, 0.0002] for the faster signal. This demonstrates that, while the signal-to-noise ratio is identical, the faster-decaying autocorrelation results in lower uncertainty.

Should these problems be solved (SNR and/or bitrate) There is yet another issue of station inaccuracies in transmission (internal delays that cannot be predicted or fixed initially due to unregulated installation cable lengths, and environmental effects on the antenna that alter its properties, thus inducing delays).

3.3.1 Introduction of the CW1 and CW2 and phase ranging

Any addendum to the system should be placed at the 0s of the spectrum of the MSK (to not interfere with the RTCM system that is already instored), and within the allocated bandwidth (to not interfere with neighboring stations in the spectrum). The zeroes of the PSD (in baseband) are at frequencies $\Delta f = \pm 25 \times (2n+1)$ with n $\epsilon[0..\infty]$ (The zeroes of equation 3.3).

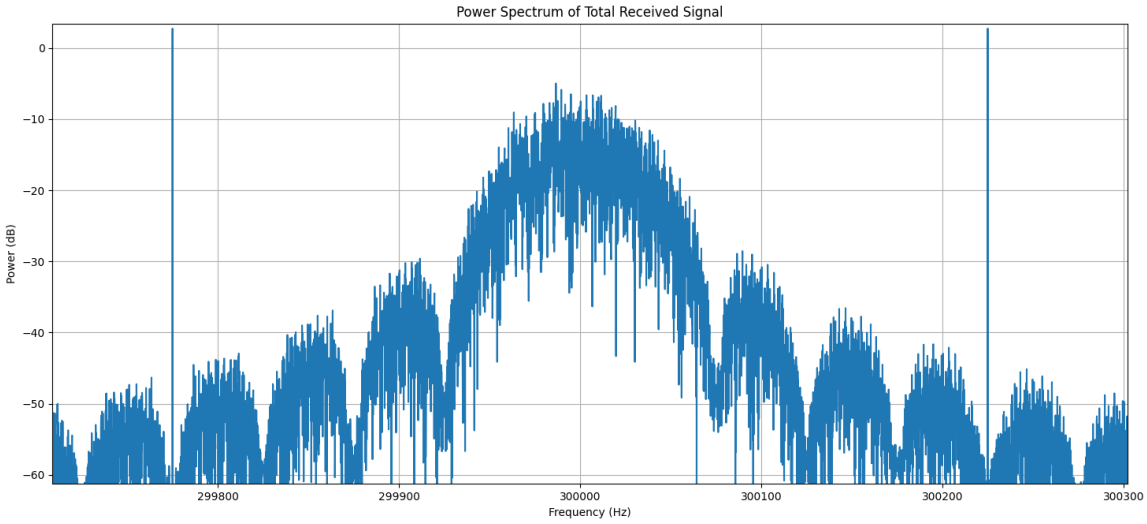

Figure 3.9: Python simulation, 2 continuous waves placed at the 4th zero of the MSK spectrum (Carrier ±225) with the CW1 at 299775Hz and the CW2 is at 300225Hz

The phase of the Continuous Wave can be leveraged to accurately estimate the distance between the transmitter and receiver.

At the receiver the wave is of the form $sin(2\pi f_c(t-\tau)) = sin(2\pi f_c t + 2\pi f_c \frac{d}{c})$ so $d = \frac{\phi \times c}{(2\pi f_c)}$ with f_c being the carrier frequency, τ is the propagation delay, ϕ is the phase perceived by the receiver and c the speed of light constant.

A single wave has an ambiguity of 1km ($\lambda_{wave} = c_{light} \times T$), with T being the period = $\frac{1}{f_c}$. 2 Continuous Waves around 308000Hz combined (added):

$$CW_1 = \sin(2\pi \times 307{,}775 \times t + \phi_1)$$

$$CW_2 = \sin(2\pi \times 308{,}225 \times t + \phi_2)$$

$$CW_1 + CW_2 = \sin\left(\frac{A+B}{2}\right) \times \cos\left(\frac{A-B}{2}\right)$$

Therefore:

$$CW_1 + CW_2 = \sin\left(2\pi \times 308{,}000 + \frac{\phi_1 + \phi_2}{2}\right) \times \cos\left(\pi \times 450 + \frac{\phi_1 - \phi_2}{2}\right)$$

form a beat wave of λ_{beat} of 666km. ϕ_1,ϕ_2 being the phase detected at the receiver side.

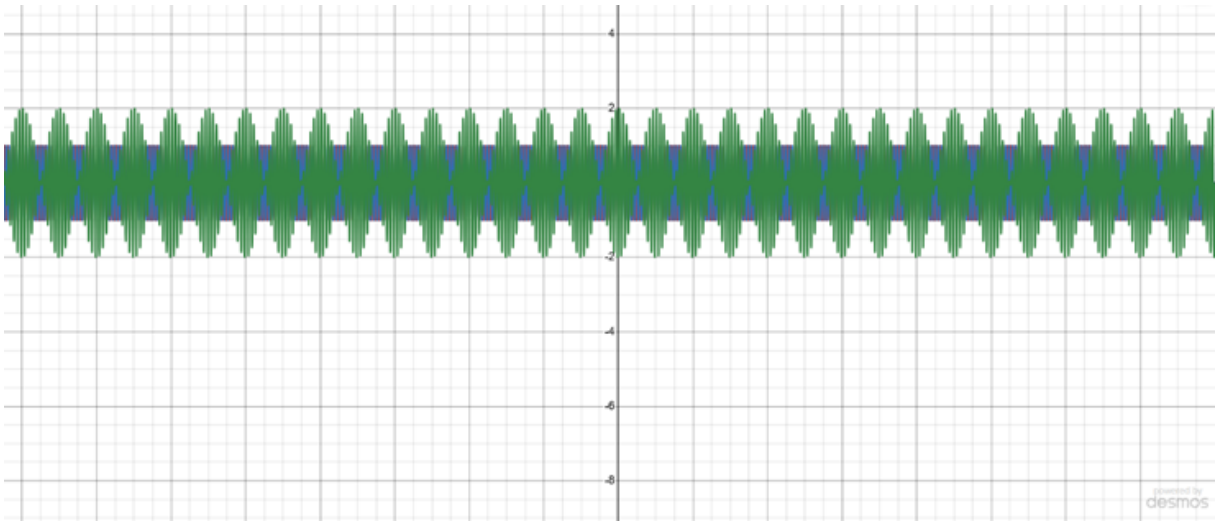

Figure 3.10: sum of Cw1 in blue, Cw2 in purple give off the beat envelope wave in Green

3.3.2 Derivation of the CRB of the phase

In this section we briefly present the results of the derivation of the lower bound for phase estimation of the beat frequency [15] The calculation is based on the Fisher Information Matrix (FIM), with parameter bounds obtained from the diagonal elements of its inverse.

$$s_{add}(t_n, \boldsymbol{\theta}) = A_1 \sin(\omega_1 t_n + \varphi_1) + A_2 \sin(\omega_2 t_n + \varphi_1 + \varphi_{beat}) \tag{3.6}$$

$$\frac{\partial s_{add}(t_n, \boldsymbol{\theta})}{\partial \varphi_1} = A_1 \cos(\omega_1 t_n + \varphi_1) + A_2 \cos(\omega_2 t_n + \varphi_1 + \varphi_{beat}) \tag{3.7}$$

$$\frac{\partial s_{add}(t_n, \boldsymbol{\theta})}{\partial \varphi_{beat}} = A_2 \cos(\omega_2 t_n + \varphi_1 + \varphi_{beat}) \tag{3.8}$$

$$\frac{\partial s_{add}(t_n, \boldsymbol{\theta})}{\partial A_1} = \sin(\omega_1 t_n + \varphi_1) \tag{3.9}$$

$$\frac{\partial s_{add}(t_n, \boldsymbol{\theta})}{\partial A_2} = \sin(\omega_2 t_n + \varphi_1 + \varphi_{beat}) \tag{3.10}$$

$$J_{add}(\boldsymbol{\theta}) = \frac{N}{2\sigma^2} \begin{pmatrix} A_1^2 + A_2^2 & 0 & 0 & A_2^2 \\ 0 & 1 & 0 & 0 \\ 0 & 0 & 1 & 0 \\ A_2^2 & 0 & 0 & A_2^2 \end{pmatrix} \tag{3.11}$$

$$J_{add}^{-1}(\boldsymbol{\theta}) = \frac{2\sigma^2}{N} \begin{pmatrix} \frac{1}{A_1^2} & 0 & 0 & -\frac{1}{A_1^2} \\ 0 & 1 & 0 & 0 \\ 0 & 0 & 1 & 0 \\ -\frac{1}{A_1^2} & 0 & 0 & \frac{1}{A_1^2 + A_2^2} \end{pmatrix} \tag{3.12}$$

$$\mathrm{var}(\varphi_1) \geq \frac{2\sigma^2}{NA_1^2} \tag{3.13}$$

$$N = T_{obs}F_s, \quad b = \frac{F_s}{2} \tag{3.14}$$

$$\mathrm{var}(\varphi_1) \geq \frac{1}{T_{obs}\, b\, \mathrm{SNR}_{A_1}} \tag{3.15}$$

$\boldsymbol{\theta}$ is the vector of parameters to estimate, namely $\boldsymbol{\theta} = [\varphi_1, A_1, A_2, \varphi_{beat}]$. ω_1 being the angular pulse of the CW_1,ω_2 the angular pulse of the CW_2, φ_1 the perceived phase of CW_1 at the receiver due to propagation delay, φ_{beat} the perceived phase of the beat wave at the receiver due to propagation delay,σ the standard deviation of the noise and A_1, A_2 being the amplitudes of CW_1 and CW_2 respectively.

In practice, plugging in a value of $T_{obs} = 1s$ and an SNR of 3dB we obtain a standard deviation of $\approx .03$ rad which equates to $\frac{c\times.03}{2\pi f_c} = \approx 3m$

We can further derive the variance of the range estimation using the beat wave

$$\varphi_1 = \frac{2\pi D}{\lambda_1} + \epsilon_1, \qquad \varphi_2 = \frac{2\pi D}{\lambda_2} + \epsilon_2 \tag{3.16}$$

$$\lambda_{beat} = \frac{1}{\frac{1}{\lambda_2} - \frac{1}{\lambda_1}} = \frac{\lambda_1\lambda_2}{|\lambda_1 - \lambda_2|} \tag{3.17}$$

$$\varphi_{beat} = \frac{2\pi D}{\lambda_{beat}} + (\epsilon_2 - \epsilon_1) \tag{3.18}$$

$$\hat{D}_{coarse} = \frac{\lambda_{beat}}{2\pi}\varphi_{beat} = D + \frac{\lambda_{beat}}{2\pi}(\epsilon_2 - \epsilon_1) \tag{3.19}$$

$$\mathrm{Var}(\epsilon_2 - \epsilon_1) = \mathrm{Var}(\epsilon_2) + \mathrm{Var}(\epsilon_1) = 2\sigma_\varphi^2 \tag{3.20}$$

$$\mathrm{Var}(\hat{D}_{coarse}) = \left(\frac{\lambda_{beat}}{2\pi}\right)^2 \cdot 2\sigma_\varphi^2 = \frac{2\lambda_{beat}^2}{(2\pi)^2}\sigma_\varphi^2 = \frac{\lambda_{beat}^2}{2\pi^2}\sigma_\varphi^2 \tag{3.21}$$

Plugging in nominal values yields a variance of 15km. The variance of the range estimate using the beat wave exceeds the wavelength of the continuous wave (i.e $\approx 1km$ by more than an order of magnitude, which prevents resolution of the phase ambiguity. Consequently, the positioning approach adopted relies on obtaining an initial fix from a known position, followed by tracking the differential phase of the continuous waves to derive delta pseudo-range updates.

In addition, phase variations may occur even (due to other external factors other than noise,without physical movement of the receiver). Such changes can result from weather-induced variations in antenna conductivity, which evolve slowly over time and therefore limit the operational period. Furthermore, station clock drift introduces additional biases that cannot be mitigated using mean square error techniques, as these biases are specific to each station rather than common across the network. As a result, each station contributes an additional unknown variable, leading to an under-determined system with insufficient equations to resolve all parameters.

Chapter 4

Contributions

As of October 2025, in parallel to the redaction of this thesis, a solution that exploits the current state of the R-Mode system has been developed latching on top of the already established work.

The current datetime value is calculated as follows:

$$datetime = timestamp + \tau_{propagation} + \tau_{transmission} - \tau_{processing} \tag{4.1}$$

Here, timestamp is the time embedded in the transmitted signal by the broadcasting station, serving as the reference for synchronization. The $\tau_{propagation}$ accounts for the travel time of the signal through the medium from the transmitter to the receiver, and is directly related to the geometric distance and propagation velocity, $\tau_{transmission}$ is indicative of the delays caused by the station itself for the signal to be physically sent through space. Finally, the processing time $\tau_{processing}$ represents internal receiver delays, such as filtering, demodulation, or hardware latency, which must be compensated to align the measurement with physical reality, and finally transmission delays concerns delays induced by the generation of the electromagnetic radiation (either at modulation, equipment, antenna properties etc..)

This formulation highlights that the receiver's estimate of the "true" current time is not simply the broadcast timestamp, but rather the timestamp adjusted for both external (propagation) and internal (processing) delays. Precise characterization of these terms is critical, since inaccuracies in propagation modeling or uncalibrated receiver delays directly degrade positioning performance.

4.1 Extracting time from MSK datastream

The process of extracting the time message from the MSK datastream involves several distinct stages, each of which is critical to obtaining a reliable and interpretable signal. From the initial demodulation to the final decoding of the message bits, every step contributes to the accurate reconstruction of the transmitted time data.

4.1.1 Reception Of Message

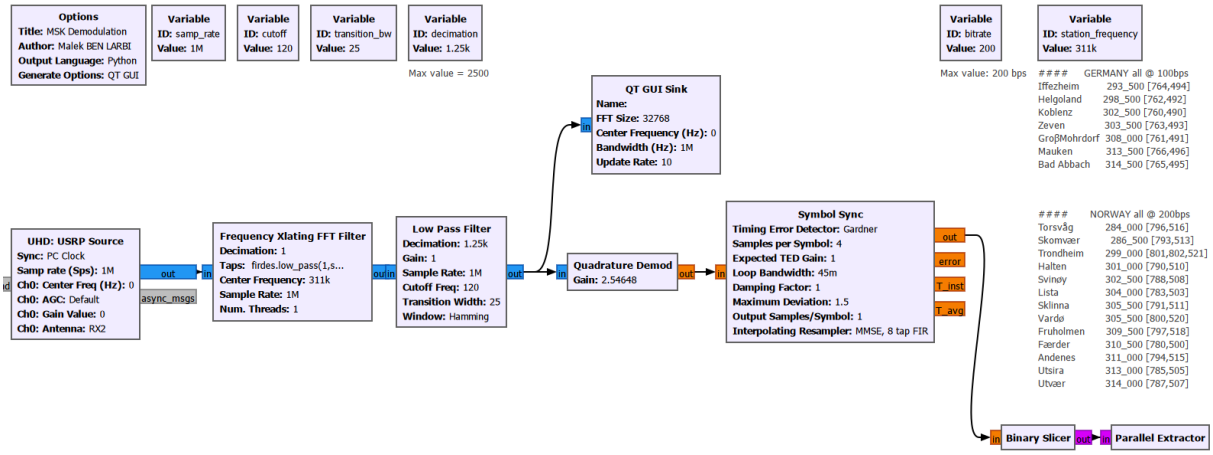

Figure 4.1: Block diagram of the GNU radio receiver

Samples go through a Frequency Translation block, then a Low pass filter, a Quadrature demodulator, a symbol synchronizer and finally a custom Python block to handle the incoming stream of bits.

4.1.2 Obtaining the Timestamp

Following the RTCM PAPER 136-2001/SC104-STD

The R-Mode DGNSS Stations broadcast an RTCMv2 formatted message.

The messages is composed of words (30 bits units).

Each word ends with 6 parity bits

The parity is calculated the same way as it is in GPS/SPS Signal specification Appendix F [16]

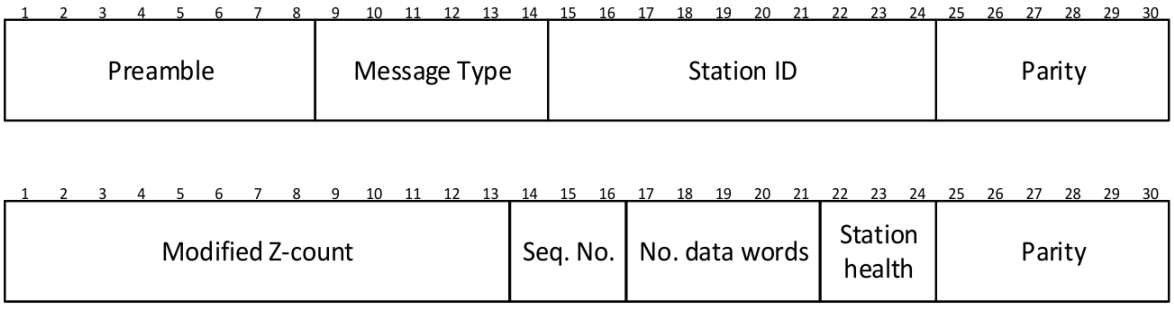

Figure 4.2: RTCM header composed of two words, time is found in the second 30-bit word of the header (from bit position 1 to 13) under the name “modified Z-count”

Our objective is to recover the z-count value stored in the second word of the header, which is considered the timestamp in equation 4.1 .

4.1.2.1 Demodulation:

Bringing to Baseband with a Frequency Translating Block: When processing a modulated signal received at a Medium Frequency, one of the first steps is down conversion or bringing the signal to baseband. This is accomplished using a frequency Xlating FFT filter (a complex local mixer).

The idea is to shift the spectrum of the received signal so that the carrier frequency is translated to zero frequency (DC), allowing for easier digital processing. Mathematically, this operation involves multiplying the input signal by a complex exponential:

$$r_{bb}(t) = r(t)e^{-j2\pi f_c t} \tag{4.2}$$

where f_c is the carrier frequency.

In the digital domain, this is implemented by multiplying the sampled data by $e^{-j2\pi f_c n T_s}$, where T_s is the sampling period. This operation shifts the desired signal to baseband while moving other frequency components (like mirror images or nearby channels) to different parts of the spectrum.

The output of the frequency translating block is thus a complex baseband signal containing both the in-phase (I) and quadrature (Q) components, ready for low-pass filtering and demodulation.

Filtering: Once the signal has been shifted to baseband, a low-pass filter (LPF) is applied to remove high-frequency components, noise, and unwanted image frequencies that are outside the bandwidth of interest.

This ensures that the filter Preserves nearly all the desired signal information. Minimizes noise contributions from outside the signal's effective bandwidth. Facilitates coherent demodulation and symbol recovery

In the case of an MSK signal of 100bps, the filter is designed to pass frequencies within a bandwidth of ±60 Hz, which implies that the useful signal energy is concentrated in that narrow band. The integration of the PSD (equation 3.4) , approximately 99% of the signal's total power lies within this ±60 Hz range. However, one can go beyond the 60hz bandwidth if doing so allows more useful signal power in the system than noise.

We can therefore programmatically adjust the bandwidth by comparing the value of the PSD to that of the noise floor.

Low-pass filtering is a prerequisite to the decimation process, ensuring that all frequency components above the new Nyquist frequency are effectively attenuated before downsampling. This preemptive filtering is crucial to prevent aliasing, a phenomenon where high-frequency components fold back into the lower frequency spectrum, distorting the signal. [17]

Without decimation, the receiver is required to process every sample at the original high sampling rate, leading to significant increases in computational load, memory usage, and data bandwidth requirements. Such high-throughput processing can exceed the capabilities of real-time hardware, such as CPUs or DSPs, resulting in unacceptable latency, missed deadlines, or dropped samples.

Decimation mitigates these constraints by selectively discarding redundant high-rate samples while preserving the essential information content of the signal. This reduction in sample rate decreases the amount of data to be processed, stored, or transmitted, thereby optimizing system performance since decimation by a factor M reduces the sampling rate by M accelerating the workflow of the subsequent blocks.

Decoding the MSK modulated signal While any two distinct frequencies F_0 and F_1 can be used for communication, designing the receiver is simplified when the tones constituting the MSK signal are **orthogonal**, meaning:

$$\int_0^{T_b} s_1(t)s_0(t)\,dt = 0$$

We shall study the frequency separation ΔF. This parameter is important for spectral efficiency, as closer frequencies allow more channels to be transmitted within the same bandwidth.

For a BFSK signal, the orthogonality condition becomes:

$$\int_0^{T_b} \cos(2\pi F_1 t)\cos(2\pi F_0 t)\,dt = 0$$

Expanding this using trigonometric identities gives:

$$\frac{\sin\left[2\pi(F_1+F_0)T_b\right]}{2\pi(F_1+F_0)} + \frac{\sin\left[2\pi(F_1-F_0)T_b\right]}{2\pi(F_1-F_0)} = 0$$

Since $F_1 + F_0 = 2F_c \gg 1$, the first term approaches zero, leaving:

$$\sin\left[2\pi(F_1-F_0)T_b\right] = 0$$

This holds when:

$$F_1 - F_0 = \frac{k}{2T_b}, \quad k \in \mathbb{Z}$$

Thus, the **minimum frequency separation** for orthogonal signaling occurs at $k = 1$:

$$F_1 - F_0 = \frac{1}{2T_b} = \frac{R_b}{2}, \quad \Rightarrow \quad \Delta F = \frac{F_1 - F_0}{2} = \frac{R_b}{4}$$

Using the minimum tone spacing above, a BFSK signal can be written as:

$$s(t) = A\cos\left[2\pi(F_c \pm \frac{R_b}{4})t\right] = A\cos\left[2\pi F_c t \pm 2\pi\frac{R_b}{4}t\right], \quad 0 \le t \le T_b$$

This represents a **continuous-phase BFSK (CP-BFSK)** signal over a single bit interval.

In practice, a communication system transmits a sequence of bits $b_n \in \{0, 1\}$, mapped to symbols $a_n \in \{-1, +1\}$. For the interval $nT_b \le t \le (n+1)T_b$, the signal is:

$$s(t) = A\cos\left[2\pi F_c t + 2\pi a_n \frac{R_b}{4}(t - nT_b)\right]$$

Here, phase continuity between symbols is not automatically guaranteed. To enforce continuity, a phase term θ_n is added:

$$s(t) = A\cos\left[2\pi F_c t + 2\pi a_n \frac{R_b}{4}(t - nT_b) + \theta_n\right]$$

The phase of the baseband signal is therefore:

$$\phi(t) = 2\pi F_c t + 2\pi a_n \frac{R_b}{4}(t - nT_b) + \theta_n$$

Taking the derivative of the phase with respect to time yields:

$$\frac{d\phi(t)}{dt} = 2\pi a_n \frac{R_b}{4}, \quad \text{with } a_n \in \{-1, +1\}$$

Finally, the value of the bit a_n can be determined from the **sign of the derivative of the phase.**

4.1.2.2 Choice synchronization method: Gardner Method

The Gardner Timing Error Detector creates a Timing Error Discriminator by estimating the derivative of the waveform at the assumed zero crossing and multiplying it by the actual sample value at that crossing. (The difference equation $y[2n+1]-y[2n-1]$ serveing as an approximation of the derivative.)

The Gardner method effectively functions as a discriminator by multiplying the waveform with its derivative, as illustrated in the two accompanying graphics.

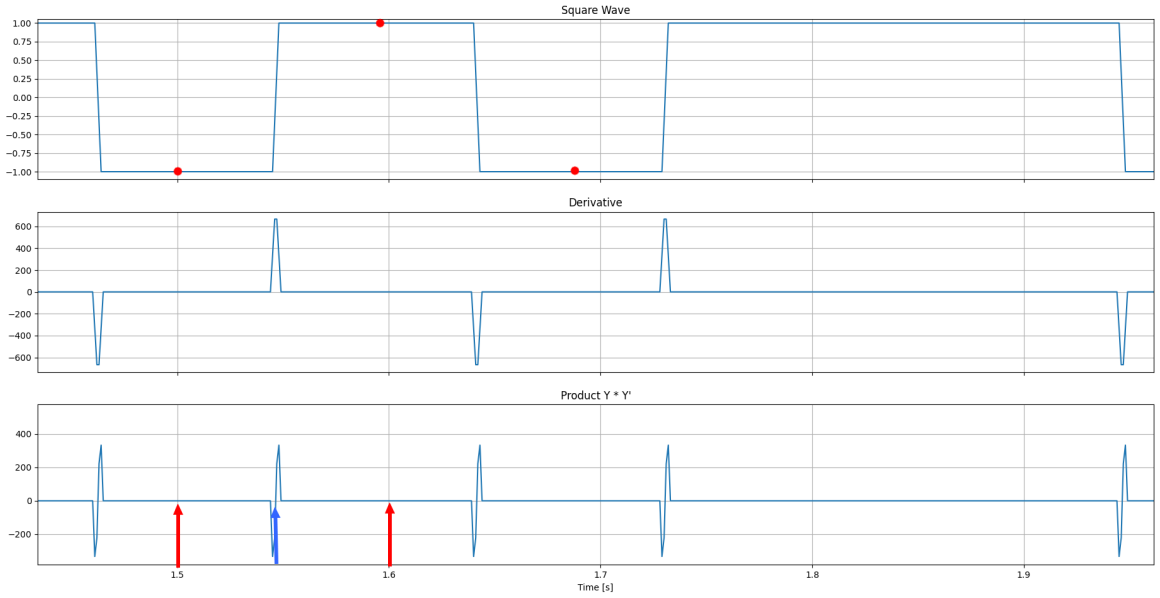

Figure 4.3: example scenario with 2 samples per symbol (red dots) Top graph is the square signal, middle is the derivative and bottom is the product of the two

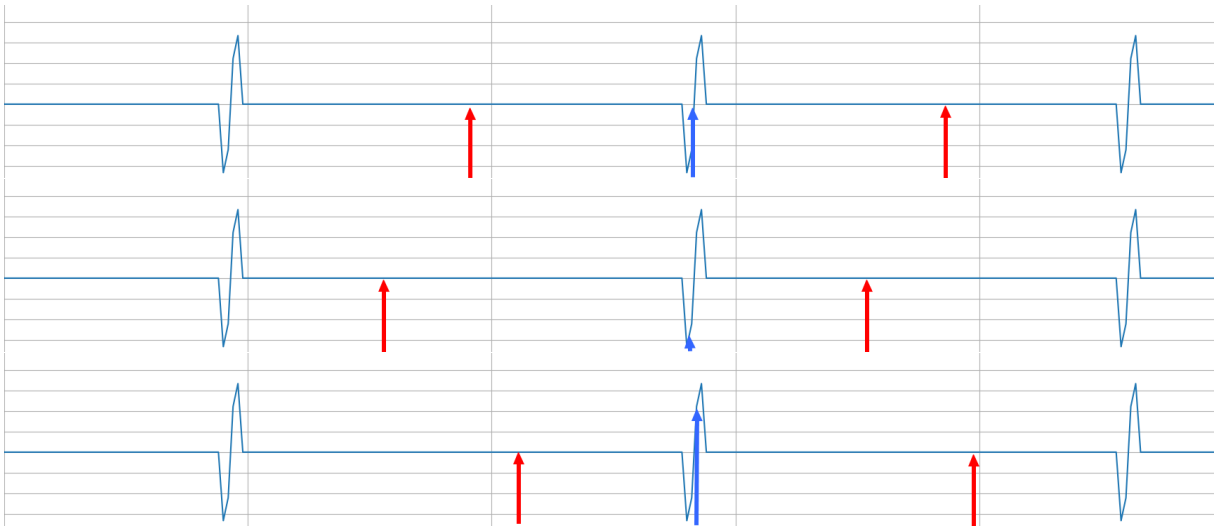

Figure 4.4: Focus on the product of the square wave and derivative (blue arrow value). Depending on the samples position, the product can be null, negative or positive.

Using the Gardner discriminator to find the optimal sampling point (If positive, then the mid sample is too late, if negative then too early)

By comparison, the Early-Late gate method estimates the derivative at the peak correlation of the data symbol. When timing is properly aligned using the Early-Late gate, the Early and Late samples fall on either side of the peak correlation, each representing a fraction of the data symbol. These samples can be spaced half a symbol apart like the Gardner approach,but the primary distinction lies in the lock point of the central sample.

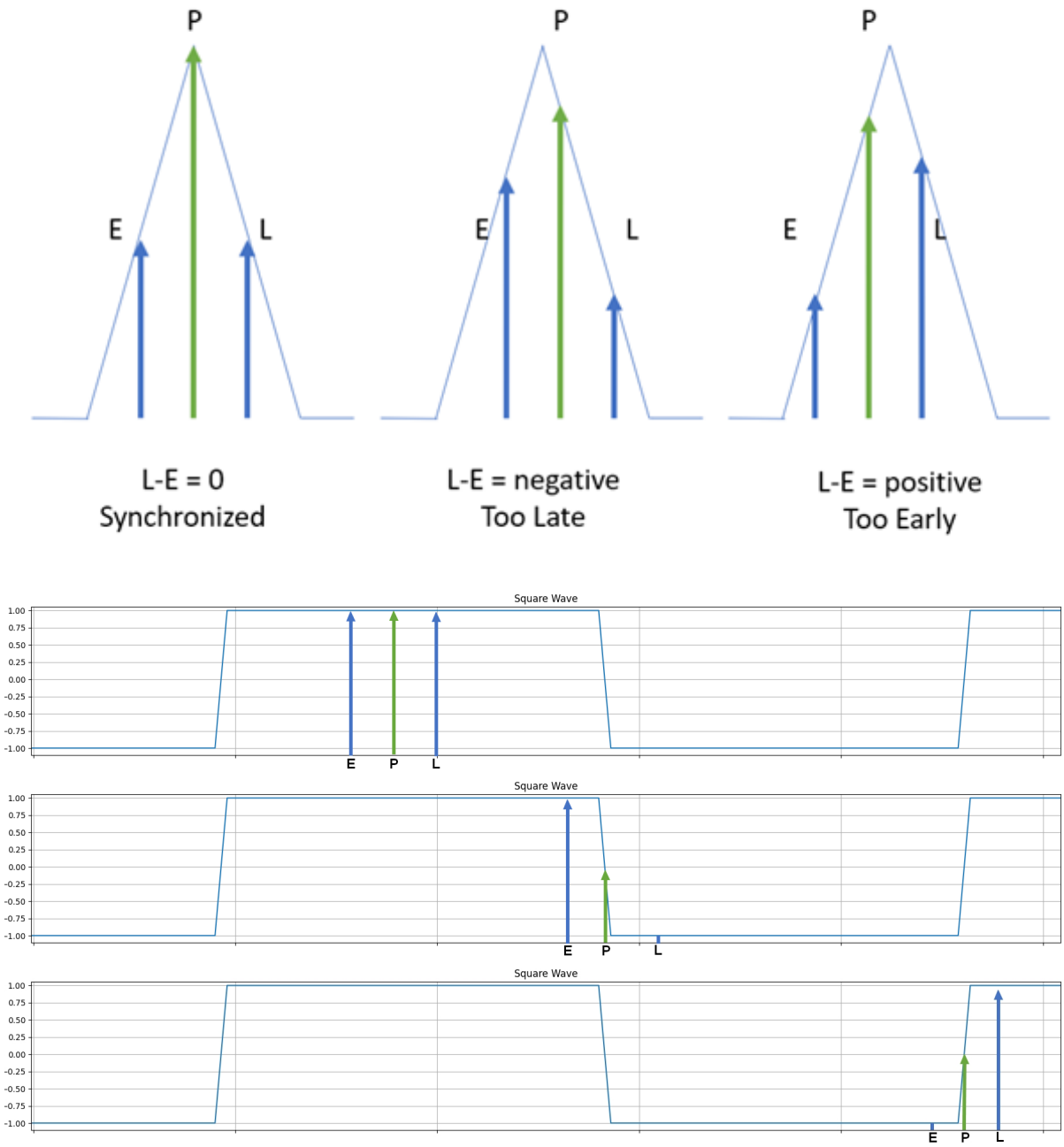

Figure 4.5: Early Late in triangle shape signal (top graph).in the context of a square wave (rest), E, P and L values are not indicative of whether the samples are early on time or late

Square waves contain flat regions between transitions (Top graph of figure 4.5). Peak-based methods rely on sampling near the symbol peak, which, in square waves, provides little timing information because the slope is zero (flat) in these regions.

In regions where the slope is not zero (Middle graph has a negative slope and bottom graph is positive slope), the discriminator is not indicative of whether or not the sample is late or early (Decision based on value).

4.1.3 Finding the word start

In the processing chain, the incoming data stream is first interpreted as a continuous stream of binary symbols (bits).

The initial step in this process involves detecting the preamble, which serves as a known reference pattern within the RTCM v2 data structure (bits 1 to 8, see figure 4.2). The preamble is a specific bit sequence defined in the RTCM documentation, and it marks the beginning of a new frame within the data stream. In RTCMv2 which this thesis deals with has a preamble of the form [0, 1, 1, 0, 0, 1, 1, 0]

Once the preamble sequence is successfully detected the receiver begins capturing the subsequent bits that constitute one complete navigation word (30 bits) fed to a custom block (Parallel Extractor in Figure 4.1).

The receiver then compares the calculated parity with the received parity bits to ensure that the word has been received correctly and that no bit errors occurred during demodulation or transmission.

If the parity check passes, confirming the word's correctness, the receiver proceeds to interpret the word's content. In this context, one of the first pieces of information examined is the Station ID (bit 15 to 24, see Figure 4.2) or the identifier of the transmitting station. The receiver verifies that this Station ID corresponds to a valid and expected value (as agreed upon, available in the IALA document [5]), consistent with the set of identifiers defined by the IALA table of DGNSS stations.

19 GERMANY

Table of DGNSS Stations			Country: GERMANY				Date of issue: January 2002 Date of last update: November 2014				
Station name	Identification Numbers		Geographical Position Latitude Longitude (WGS84)	Nominal range		Station in operation	Integrity Monitoring	Transmitted message types	Freq. (kHz)	Bit Rate (bps)	Remarks
	Reference Stations	Transmitting Station		Km	at (µV/m)						
Helgoland	762	492	54° 11′ N 007° 53′ E	285	50	Yes	Yes	3 6 7 9 16	298.5	100	
Koblenz	760	490	50° 22′ N 007° 38′ E	225	50	Yes	Yes	3 6 7 9 16	302.5	100	
Zeven	763	493	53° 17′ N 009° 15′ E	285	50	Yes	Yes	3 6 7 9 16	303.5	100	
GroßMohrdorf	761	491	54° 22′ N 012° 55′ E	285	50	Yes	Yes	3 6 7 9 16	308.0	100	
Iffezheim	764	494	48° 50′ N 008° 07′ E	225	50	Yes	Yes	3 6 7 9 16	293.5	100	
Bad Abbach	765	495	48° 56′ N 012° 02′ E	225	50	Yes	Yes	3 6 7 9 16	314.5	100	
Mauken	766	496	51° 43′ N 012° 49′ E	225	50	Yes	Yes	3 6 7 9 16	313.5	100	

Table 4.1: A list of the German DGNSS stations [5]

4.1.4 In practice

To better illustrate the overall decoding and validation process, we shall consider the practical example of the Heligoland station, seen in table 19 of the IALA DGNSS station document which serves as one of the reference and transmission sites within the differential GPS (DGPS) network.

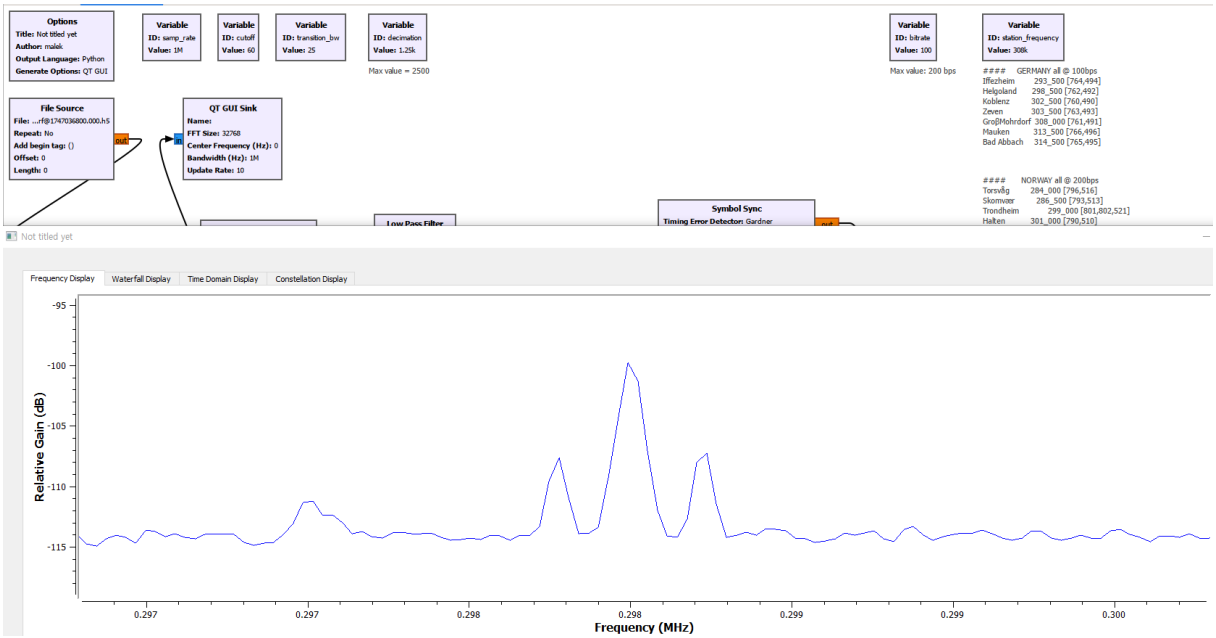

Figure 4.6: Zoom on the spectrum, the Heligoland station 298.5khz is visible with its central MSK broadcast and two continuous waves to its left and right.

The first step consists in down conversion by the precise carrier frequency associated with this station, which in this case is 298.5 kHz. This frequency lies within the LF (Low-Frequency) radio band typically used for DGPS data broadcasts. By setting the receiver's local oscillator to this frequency and multiplying the incoming complex signal, the incoming RF signal is translated to baseband, making it suitable for subsequent digital processing.

It is not necessary to consider compensating for the doppler shift as the value is insignificant

$$\frac{\Delta f}{f} = \frac{v}{c}$$

(Vessels moving at 30 km/h will shift the 300 kHz wave by approximately ±0.008 Hz. And an airplane at 1000 km/h will experience a ±.27hz shift)

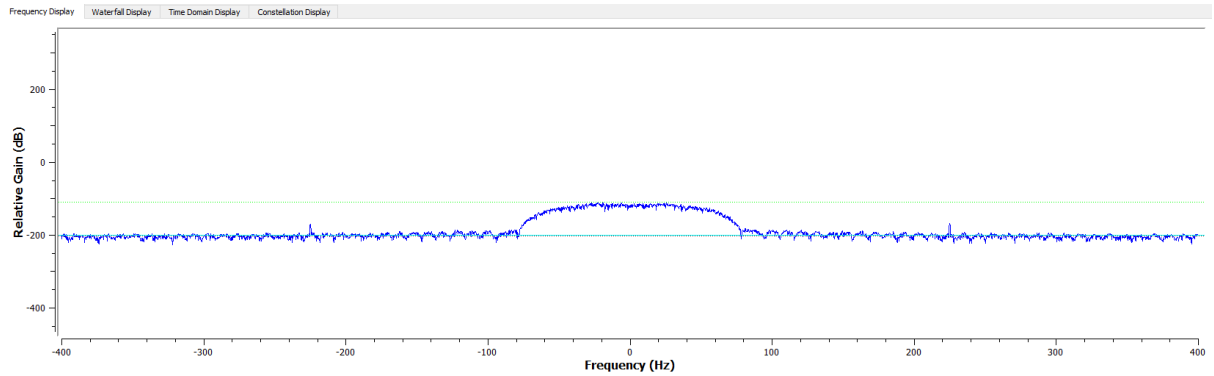

Figure 4.7: Down conversion and filtering, both the continuous at ±225hz waves see their power drastically decrease since they are out of the bandwidth of interest

Once tuned, the receiver applies a low-pass filter of 60hz bandwidth to isolate the desired signal and suppress unwanted spectral components and noise outside the channel of interest. The filter

bandwidth is carefully chosen to preserve the essential modulation characteristics while minimizing interference from neighboring frequencies. This filtering stage is crucial for maintaining a high signal-to-noise ratio (SNR), which directly affects the reliability of bit detection in later stages.

Following filtering, the demodulation process begins. The received signal, which is encoded in the phase must be tracked to correctly recover the embedded binary data. the demodulator will then convert converts phase transitions into discrete binary values, thereby reconstructing the underlying bit stream.

At this stage, the receiver continuously processes this stream of bits in real time while monitoring the presence of a preamble sequence. The preamble is a well-defined binary pattern, standardized according to RTCM specifications, and it serves as a marker for word or frame synchronization. By correlating the incoming bit stream with the known preamble sequence, the receiver can identify the start of a new data word or message frame.

When the preamble is detected, the system aligns its internal timing accordingly and begins to collect the subsequent bits that form the first header word. Each word consists of 30 bits, comprising both 24 data bits and 6 parity bits used for error detection. The receiver performs a parity check based on the algorithm described in the GPS Standard Positioning Service (SPS) documentation. This check involves computing expected parity values from the received data bits and comparing them to the transmitted parity bits. A mismatch indicates that one or more bits have been corrupted during transmission, while a match confirms the integrity of the word.

$$
\begin{aligned}
D_1 &= d_1 \oplus D^*_{30} \\
D_2 &= d_2 \oplus D^*_{30} \\
D_3 &= d_3 \oplus D^*_{30} \\
&\bullet \quad \bullet \\
&\bullet \quad \bullet \\
&\bullet \quad \bullet \\
&\bullet \quad \bullet \\
D_{24} &= d_{24} \oplus D^*_{30} \\
D_{25} &= D^*_{29} \oplus d_1 \oplus d_2 \oplus d_3 \oplus d_5 \oplus d_6 \oplus d_{10} \oplus d_{11} \oplus d_{12} \oplus d_{13} \oplus d_{14} \oplus d_{17} \oplus d_{18} \oplus d_{20} \oplus d_{23} \\
D_{26} &= D^*_{30} \oplus d_2 \oplus d_3 \oplus d_4 \oplus d_6 \oplus d_7 \oplus d_{11} \oplus d_{12} \oplus d_{13} \oplus d_{14} \oplus d_{15} \oplus d_{18} \oplus d_{19} \oplus d_{21} \oplus d_{24} \\
D_{27} &= D^*_{29} \oplus d_1 \oplus d_3 \oplus d_4 \oplus d_5 \oplus d_7 \oplus d_8 \oplus d_{12} \oplus d_{13} \oplus d_{14} \oplus d_{15} \oplus d_{16} \oplus d_{19} \oplus d_{20} \oplus d_{22} \\
D_{28} &= D^*_{30} \oplus d_2 \oplus d_4 \oplus d_5 \oplus d_6 \oplus d_8 \oplus d_9 \oplus d_{13} \oplus d_{14} \oplus d_{15} \oplus d_{16} \oplus d_{17} \oplus d_{20} \oplus d_{21} \oplus d_{23} \\
D_{29} &= D^*_{30} \oplus d_1 \oplus d_3 \oplus d_5 \oplus d_6 \oplus d_7 \oplus d_9 \oplus d_{10} \oplus d_{14} \oplus d_{15} \oplus d_{16} \oplus d_{17} \oplus d_{18} \oplus d_{21} \oplus d_{22} \oplus d_{24} \\
D_{30} &= D^*_{29} \oplus d_3 \oplus d_5 \oplus d_6 \oplus d_8 \oplus d_9 \oplus d_{10} \oplus d_{11} \oplus d_{13} \oplus d_{15} \oplus d_{19} \oplus d_{22} \oplus d_{23} \oplus d_{24}
\end{aligned}
$$

where:

$d_1, d_2, \cdots d_{24}$ are the source data bits

the symbol (*) is used to identify the last 2 bits of the previous word of the subframe,

$D_{25}, \cdots D_{30}$ are the computed parity bits

$D_1, D_2, D_3, \cdots D_{29}, D_{30}$ are the bits transmitted by the satellite, and

$\oplus$ is the "Modulo-2" or "Exclusive-Or" operation.

Figure 4.8: GPS SPS algorithm of parity checking

After successful parity verification, the receiver proceeds to interpret the contents of the header word. One of the first fields to be examined is the Station ID, which identifies the transmitting or originating station.

If the extracted Station ID matches one of these values of an entry of the IALA table (simlar to figur 4.6), the word is considered valid and can be processed further. However, any deviation from these expected identifiers (e.g valid ID at a wrong channel) is a clear indication of an erroneous message. Such discrepancies may arise from bit errors, incorrect synchronization, or interference from another transmission source. In these cases, the receiver must discard the word and resume searching for the next valid preamble to reestablish proper reception of messages.

By following this step-by-step approach tuning, filtering, phase tracking, preamble detection, parity verification, and station ID validation the receiver ensures that only authentic and error-free messages are retained for decoding. This careful validation process safeguards the reliability of the differential corrections and ensures that the positioning data derived from the Heligoland station remain both accurate and trustworthy.

4.1.5 Identification of miscellaneous problems

As previously mentioned, the MSK time stamp is currently only 13 bit long, with a resolution of .6s (i.e we have a total resolution of $8192 \times 0.6s = 4915.2s = 1h21min55.2s$

If an initial fix is given, then the system can continuously build upon it and update its current time, in a way that matches the incrementation of the z-count.

However, this setup is not sufficient if the system is meant to start from 0 (cold start) while needing full Year, Month Day Hours Minutes and Seconds (for the purposes specified in 1.4)

Some Errors may arise from the fact that the timestamp is not initially designed to indicate the correct real time but rather is used for correction purposes (to be plugged into correcting equations see RTCM Teil a) the bit start sometimes aligns with the correct time, but it is not a requirement/not guaranteed.

Plus, even if it were engineered to indicate the current time, station conditions (delays induced by the modulation step, or weather conditions affecting the properties of the transmitting antenna) are undetermined, therefore transmission is off by an unknown factor

The processing time in the local receiver is also nondeterministic, different in each execution due to the unpredictable nature of scheduling on normal operating systems. (Need for a real time deterministic operating system RTOS)

4.1.6 Propagation Delay

The positioning aspect itself lies beyond the primary scope of this thesis, as the main focus here is on the application of the derived data for time synchronization rather than on the positioning process per se.

Nevertheless, it is worth mentionning that this section has been studied in-depth [18] based on the results obtained in Section Estimation of the phase under gaussian noise, the positioning accuracy achievable with the employed R-Mode configuration is on the order of the meter.

Although this level of uncertainty is relatively small, it nonetheless establishes a fundamental lower bound on the achievable timing precision under gaussian noise (i.e an uncertainty of 10m translates to an uncertainty of $\frac{10}{c} \approx 33.3ns$ with c the speed of light).

4.1.7 Processing time

The Continuous waves and the square wave generated by the station should all share the same 0 since they are generated and managed by the same reference clock.

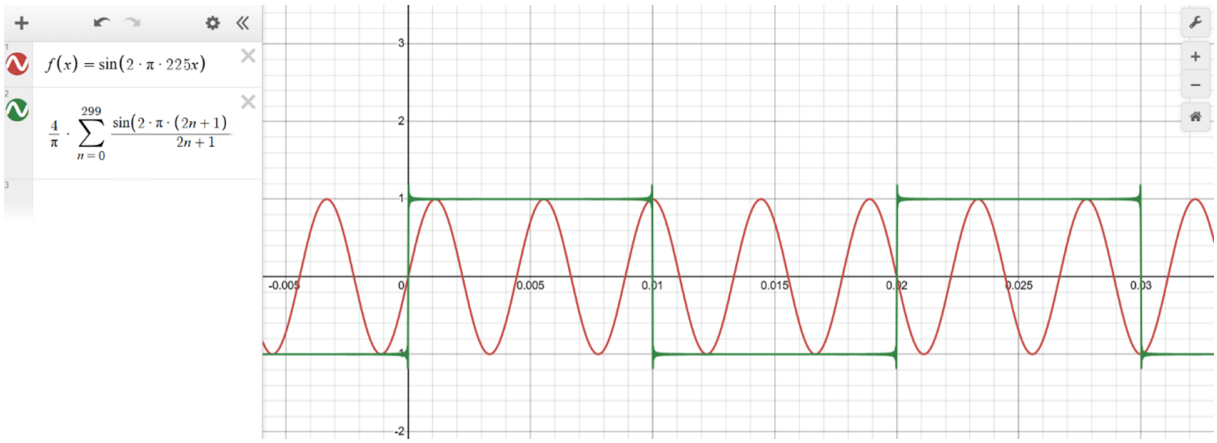

Figure 4.9: Thecontinuous wave (red) and the square wave (green) generated by an R-Mode station in baseband: The phase at t=0 is zero. The start of the bit aligns with t=0

Every bit of the MSK transmission has a duration of .01s.

At the end of the duration of 1 bit, the phase of the continuous wave

$$sin(2 \times \pi \times 225(t + .01)) = sin(2 \times \pi \times 225t + \frac{\pi}{2})$$

would've evolved by $\frac{\pi}{2}$.

Therefore the end/start of an MSK bit aligns with a phase of either 0, $\frac{\pi}{2}$, $-\frac{\pi}{2}$ $[2\pi]$ of the continuous wave.

Since words are 30 bits long, we expect the phase at the end of transmission of each word to be $30 \times \frac{\pi}{2} = 15\pi \equiv \pi[2\pi]$ which means that the phase of the continuous wave is always either 0 or $\pi[2\pi]$ at the time the last bit of a word is sent.

We can exploit this property to try and estimate the start of any bit and potentially obtain the processing time.

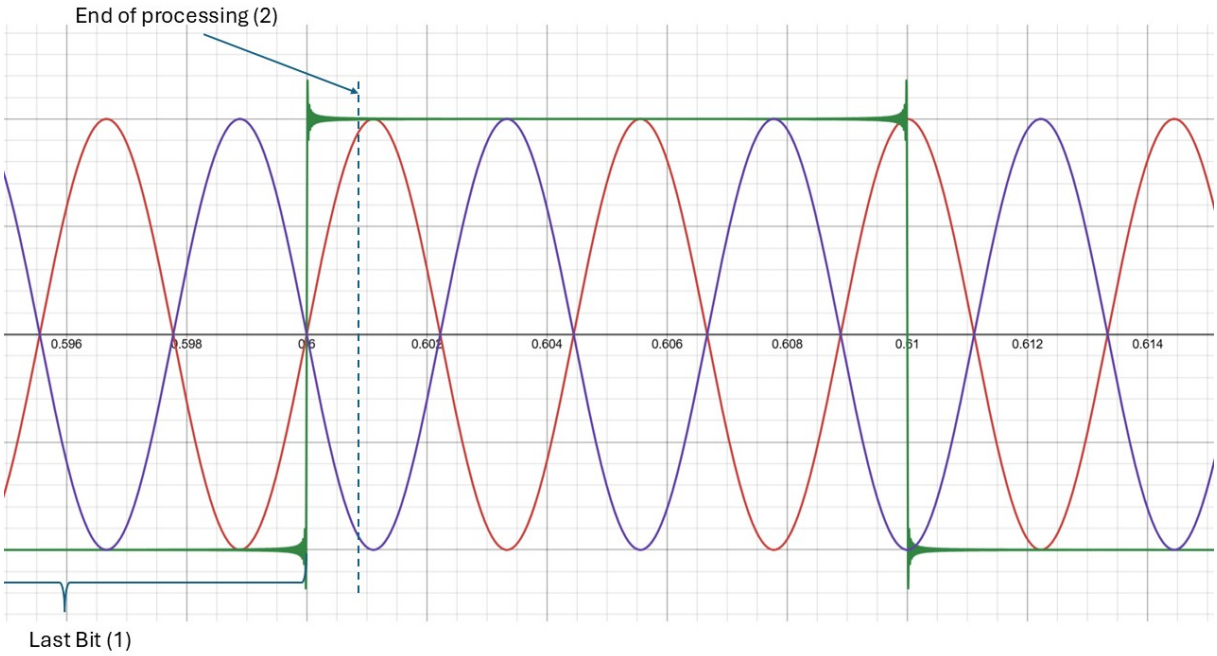

Figure 4.10: after the reception of the last bit (1) and the end of the decoding of the message (2) the phase of the continuous wave would have evolved to a new value $\varphi \neq 0[\pi]$

The formula for the elapsed time is given by

$$\frac{\varphi[mod\pi]}{2\pi 255}. \tag{4.3}$$

where φ is the measured phase.

One can argue that that the above mentioned procedure of estimating the processing time is also itself a process of its own, however:

"Looking" at the current phase at the end of the processing has a time complexity C(1). (i.e Atomic operation = considered instant = causes no delay 1 clock cycle)

And Multiplying the phase by the angular frequency could also be considered atomic operations (Although floating point arithmetic is notoriously slow, usually taking up to 4 clock cycles = 1.33 nanoseconds taking as an example a mainstream chip architecture [19]

It is also acceptable that the process gets scheduled by the operating system (starts) at a random time so long as we guarantee it is triggered within 1/450s. Failing to do so will lead to an estimation is ambiguous since it is 1/450s periodic (as the phase reading is itself pi periodic).

4.2 Future improvements (the addition of Message 55 per station)

The introduction of Message 55 within the IALA Guideline G1187 marks a decisive step toward the operational maturity of the R-Mode navigation system. It brings a flexible structure consisting of a standard RTCM header followed by an R-Mode-specific header and up to six well-defined submessages. This modular design allows both static and dynamic data to be transmitted efficiently, ensuring that critical information (such as station health, timing offsets, and correction

data) reaches the user with appropriate frequency and reliability. The message integrates seamlessly with legacy Differential GNSS transmissions, allowing both services to coexist without impairing existing GNSS correction broadcasts. Among the major contributions of Message 55 is the establishment of a traceable time reference through the R-Mode System Time, a realization of UTC (namely RMST) maintained across the R-Mode network. The message provides parameters for converting RMST to UTC, managing leap seconds, and monitoring station clock synchronization. This time integrity ensures interoperability between R-Mode and GNSS systems, allowing navigators to fuse terrestrial and satellite data into a single, coherent positioning solution. Further innovations appear in the submessages introduced by Message 55. Submessage 1 delivers precise timing information, clock offsets, and signal delays for the three MF R-Mode signal components (MSK and two CWs). Submessage 2 conveys static data such as transmitter coordinates and carrier characteristics, enabling accurate geometric modeling. Submessage 3 provides RMST-to-UTC conversion data, while Submessage 4 supports continuity during synchronization outages by modeling free-running clock behavior. The optional Submessages 5 and 6 introduce the Differential R-Mode concept,localized corrections and integrity indicators that improve accuracy and reliability, particularly in coastal or harbor environments where propagation effects are variable.

4.2.1 Synchronized, Coordinated Emission of Message 55

A central promise in G1187 is that all R-Mode stations are made to emit messages in a synchronized, coordinated manner, tied to the R-Mode System Time (RMST). This is critical for moving receivers, and although less demanding for stationary receivers, it still contributes to coherence and system integrity.

One of the key advances in the IALA G1187 specification is that Message 55 (or the R-Mode navigation message) is designed to explicitly carry information about the timing of each transmitted signal component, including the delay of each component and a phase value for the MSK (Minimum Shift Keying) signal component. In other words, rather than relying solely on receiver-side assumptions or generic calibrations, the system enables per-station, per-component delay calibration. [20] p.21.

This feature addresses a longstanding challenge in radio-based ranging systems: the fact that a transmitter's internal chain (filtering, modulation, buffering, switching, amplifier delays, antenna feed lines, etc.) introduces a non-negligible and often time-varying offset between the nominal "transmit time reference" and the actual radiated signal. Some of these delays cannot be compensated for by other means (i.e., they are intrinsic to the hardware and path) unless they are measured and reported. The inclusion of these delay terms in the message ensures that the receiver can subtract them explicitly, thereby removing a source of systematic bias in time-of-arrival (ToA) estimation.

By decomposing the station delay into subcomponents (for example, lead-in filter delay, modulation latency, buffer latency, switch or antenna feed delay), and broadcasting phase offsets for MSK bit transitions, the system allows:

Better relative alignment: because each station is synchronized to the R-Mode System Time (RMST), having per-component delay calibration ensures alignment not just in coarse time, but in the micro- or nanosecond domain across multiple stations.

In effect, the message enables the receiver to reconstruct, more precisely:

where is the reported station delays. This allows the receiver to reduce or eliminate bias errors that would otherwise remain if station delay were only corrected by a blanket offset or ignored.

From a design perspective, this capability necessitates that the transmitting station continuously calibrates or monitors its internal delays and embed updated values in subsequent messages, especially if hardware conditions (e.g. temperature, humidity, aging of components) change over time.

This approach solves the problem of individual, specific station delays by shifting the burden of accurate measurement to the transmitter side and empowers the receiver to use those calibrated values rather than approximate or generic corrections.

4.2.1.1 Why synchronized transmission matters

G1187 defines that the aligning features of the signal (e.g. the zero crossing of aiding carriers, the timing of MSK bit transitions) are referenced to RMST, and any deviations from ideal timing are made known in the R-Mode navigation message.

Thus, ideally, each station's transmit waveform is phase-locked in time and aligned to an absolute second boundary in RMST. Real-world deviations due to hardware or propagation must then be reported, but the baseline is that all stations share a common temporal reference.

To realize this, each station must maintain a high-precision time reference (e.g. rubidium or better clocks), disciplined by GNSS or another high-stability source, but kept free from transient errors.

Station controllers receive RMST updates and schedule transmissions accordingly. Any latency or jitter in the control link must be minimized.

Even between synchronization epochs, small drift or jitter may occur. G1187's mechanism of per-message delay offsets helps to absorb and correct residual misalignments.

A moving receiver, by assuming the station emissions are aligned, can reliably attribute arrival offsets to geometry and propagation, rather than having to estimate inter-station synchrony. This simplifies the receiver's calibration burden and reduces error covariance.

Even for stationary receivers, synchronized transmissions help reduce temporal drift in the system and ensure uniformity of the ranging network.

4.2.2 Propagation Map / Space-Delay Correction via Conductivity Variation

G1187 also introduces the concept of a propagation map [20]p28, to compensate for space-dependent delays due to varying ground conductivity along the propagation path. Because MF radio signals propagate as groundwave across the Earth's surface (and slightly above), the effective velocity and path curvature (and thus the time delay) are influenced by local environmental properties, particularly the conductivity and permittivity of the medium (seawater, coastal sediments, sea/land interface).

4.2.2.1 Why is a propagation map needed

The effective velocity is not constant over the path. In regions with higher conductivity, the groundwave attenuation is lower, and propagation is slightly faster (less dispersion). Conversely, in lower-conductivity regions (e.g. land, wetlands, varying geology), the propagation slows.

Coastal zones often involve transitions from sea to land, sediment layers, varying bathymetry, and

inhomogeneous conductivity. These create local anomalies in propagation delay which contribute to range and time error bias.

The specification calls for the inclusion of a propagation delay correction map, effectively a spatial grid or model, which the receiver or base processing can use to compute differential delay corrections along the expected path between station and receiver. This map is intended to be specific to each transmitting station's coverage area, and could include parameters such as conductivity gradients, terrain or land mask corrections, and path-integrated effective velocity deviations.

More precisely, for a given station and a receiver position estimate, one would compute:

where is a path coordinate and is a nominal reference velocity. The propagation map provides a lookup or interpolation table for corrections depending on path geometry.

Under real operation, this means:

As the receiver refines its position (via tri/multilateration), it also refines the path integral through the conductivity map for each link, and updates propagation delay accordingly.

The propagation corrections may be precomputed for a grid of positions relative to each station and included in the navigation message (via an ID, as indicated on page 28) and stored locally in the receiver.

The map can also allow updates over time if conductivity (salinity, temperature) or environmental conditions change (e.g. seasonal or weather influence on seawater conductivity) by just varying the ID value of the map.

Incorporating this correction serves to reduce systematic bias in propagation delay (especially for longer-range stations or paths crossing mixed sea/land interface zones). This improves time estimation accuracy by compensating for path-specific anomalies that raw distance-based models cannot capture.

Message 55 (as much as any other message) decoding and exploiting can be implemented on top of the already developped GNU radio solution, inside the parallel extractor block.

4.3 After the time fix

So far, as described previously in this thesis, we are capable to push a date-time value into the system's time register. At that specific instant , we can confidently assume that the time is accurate enough and synchronized with the reference. However, maintaining that accuracy over time becomes a significant challenge due to the inherent limitations of quartz-based oscillators commonly used in low-cost clock systems.

4.3.1 Quartz oscillators

Quartz oscillators form the backbone of most digital timing systems because of their simplicity, affordability, and relatively good short-term stability. They operate based on the piezoelectric properties of quartz crystals, which resonate at a precise frequency when an electric field is applied. Despite their widespread use, not all quartz oscillators are created equal. lower-cost versions often suffer from poor long-term stability and higher frequency drift. This drift refers to the gradual deviation of the oscillator's frequency from its nominal value, which directly translates into timing errors as time progresses.

In our specific case, the quartz oscillator demonstrates a drift rate of approximately 8 microseconds per second (20 seconds every month) [21]. ($\pm 100ppm$ stability on a 12MHz clock is$\equiv \frac{100}{12\times10^6} sps = \frac{100\times3600\times24\times30}{12\times10^6} = 21.6$s per month). Such inaccuracies make it clear that relying solely on an unsynchronized, free running quartz oscillator is unsuitable for applications demanding precise timekeeping or synchronization between multiple systems.

The primary sources of drift in quartz oscillators are temperature variations, aging of the crystal, mechanical stress, and voltage instability in the driving circuit. Even minor temperature changes can alter the crystal's resonant frequency, leading to measurable shifts in timing accuracy. High-quality oscillators (such as temperature-compensated crystal oscillators (TCXOs) or oven-controlled crystal oscillators (OCXOs)) mitigate these effects, but they come at a higher cost and power consumption, which may not be acceptable in all designs.

Because of this high drift rate, we must implement a correction or synchronization mechanism to maintain accurate timekeeping. One approach involves periodically re-synchronizing the system clock with a reliable external time reference, in our case, a highly stable remote oscillator (i.e the continuous wave). The method involves using the local clock to generate a signal that it assumes being is at the right frequency and mix the incoming R-Mode continuous wave. If the FFT of this mixing results in a peak at 0 then the local clock's frequency is calibrated. Any deviation from 0 should result in an increase or decrease in the local clock's frequency depending on the frequency shift.

4.3.2 Feedback loop of the clock oscillator

Any oscillator, no matter how stable, will exhibit some degree of frequency drift over time due to temperature variations, component aging, voltage fluctuations, and other environmental factors. To ensure long-term frequency accuracy, a feedback loop is implemented to monitor, detect, and correct this drift in real time. One effective way to achieve this is by using a Continuous Wave (CW) signal as a frequency reference and applying Fast Fourier Transform (FFT) analysis to estimate and compensate for deviations.

The principle of this feedback mechanism relies on comparing the locally generated oscillator signal with a known, stable CW signal received externally (by means of phase tracking or multiply one by the conjugate of the other). If we decide to track the phase then any deviation from the expected value is a clear indication of a drift. If we decide to locally mix the incomming wave with a locally generated one, we can observe the frequency spectrum and identify the peak frequency corresponding to the product. Using the CW FFT method, the precise position of this spectral peak allows us to measure the frequency offset (or deviation) from the expected nominal value. This deviation directly reflects the drift of the local oscillator relative to the reference source.

By averaging the FFT results over a defined period (typically one second) we can reduce random noise and short-term fluctuations, improving the accuracy and stability of our drift estimation.

Once the drift has been quantified (by either methods), the feedback loop can apply corrective adjustments to the oscillator's control input (such as tuning voltage in a Voltage-Controlled Oscillator or digital correction in a numerically controlled oscillator). This keeps the local oscillator locked to the external reference and significantly reduces long-term frequency errors.

An important consideration in this approach is the choice of CW reference signal. Since any continuous wave can serve as a reference, we have flexibility in selecting a signal source. However, to achieve optimal performance and minimize uncertainty, it is best to choose the CW signal with the highest Signal-to-Noise Ratio (SNR). A higher SNR ensures that the FFT peak is more distinct and less affected by background noise, allowing for more precise peak detection and thus

more accurate frequency drift estimation. Poor SNR, by contrast, can cause spectral broadening or peak ambiguity, which leads to errors in the frequency correction process.

The feedback loop of the clock oscillator can therefore function as a self-correcting mechanism that maintains timing precision through continuous monitoring and adjustment.

We can accurately measure the oscillator's drift, analyze its frequency stability over short and long-time scales, and apply real-time corrections.

Chapter 5

Results

The experimental validation of the proposed R-Mode time extraction and synchronization framework was conducted through GNU Radio testing using recorded R-Mode signals from the available R-Mode stations under normal conditions and jamming conditions. The primary objectives were to both evaluate the feasibility of timestamp recovery from Minimum Shift Keying (MSK)-modulated transmissions and quantify the short-term and long-term stability of the local oscillator when locked to a continuous-wave (CW) reference and finally assess the overall timing accuracy of the system under realistic noise and processing conditions.

5.1 Timestamp Extraction Performance

The first stage of testing focused on verifying the correct demodulation and decoding of the RTCM v2 data messages embedded in the MSK waveform. Using the GNU Radio receiver chain described previously (frequency translation → low-pass filtering → symbol synchronization → custom Python decoder), the system successfully recovered valid RTCM messages in real time.

To confirm message integrity, the receiver continuously monitored preamble detection rates, parity checks, and Station ID validation. Over multiple runs, no parity errors were observed after the first second of acquisition, indicating stable synchronization between the receiver's symbol timing and the transmitted MSK bitstream. The correct Station IDs (761 for the reference and 491 for the transmitting station) were consistently detected, confirming unambiguous source identification.

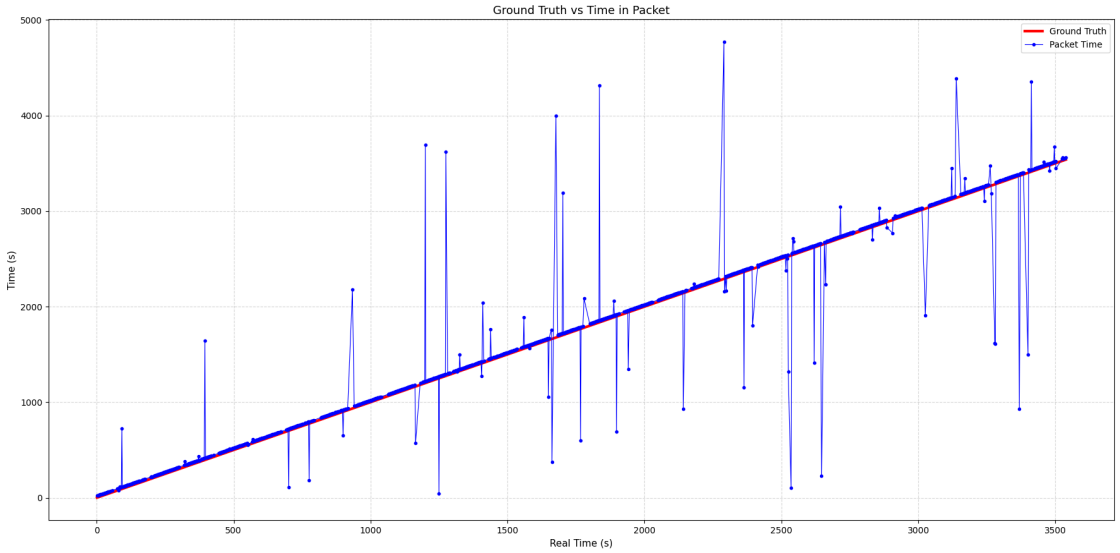

Figure 5.1: Real time value (Red line) and time value extracted from packets sent by GrossMohdorf station (Blue)

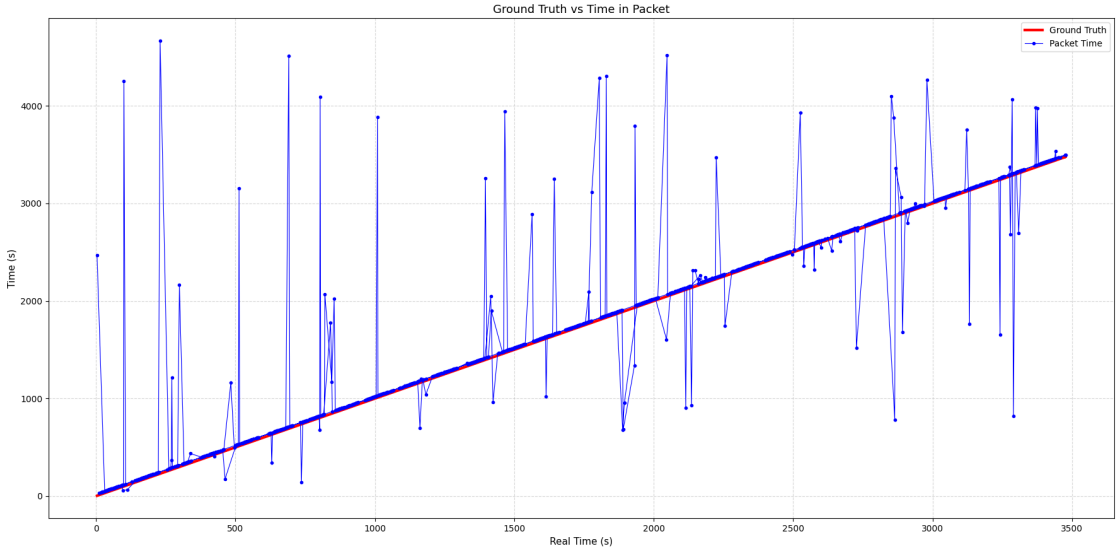

Figure 5.2: Real time value (Red line) and time value extracted from packets sent by Heligoland station (Blue)

The modified Z-count field (13 bits) was extracted from each header word, and the sequence increments also matched the expected 0.3 s multiple, defined per word length in the RTCM-104 standard . During continuous reception, the receiver successfully maintained synchronization over extended observation intervals without losing clock continuity due to our robust implementation.

However, it is worth noting that the raw packets themselves may contain unusable time data (i.e the 64 spikes deviating from the diagonal line of slope 1 in Figure 5.1 out of 1331 total packets or 4.8% error rate). and 81 spikes in Figue 5.2 (6.3% error rate) . These seemingly erroneous

packets are not due to an implementation error on the receiver side(i.e not caused at reception, and several demodulation both coherent and non coherent techniques were tested) but rather, it is data, broadcasted by the station, that is solely intended for DGNSS purposes only (i.e without the requirement to be indicative of the current time), while most other packets serve the purpose of both DGNSS corrections and timekeeping.

5.2 Continuous Wave (CW) Phase Stability

Following successful timestamp extraction, experiments were performed to analyze the stability of the continuous-wave components transmitted alongside the MSK signal. These CW tones serve as high-precision phase references used for frequency and clock stabilization.

For a convolution time of 1 second, and for the entirety of the data, the FFT analysis of the received CW signals revealed sharply defined spectral peaks at their nominal frequencies (graphically). This was due to remarkable stability of the heated rubidium frequency standard as the local oscillator reference during the measurement. Because the rubidium clock maintained thermal and voltage equilibrium throughout the test period, the FFT spectrum of the phase difference consistently exhibited a central peak at 0 Hz offset, signifying perfect lock to the CW reference. No measurable drift was detected over one-hour run.

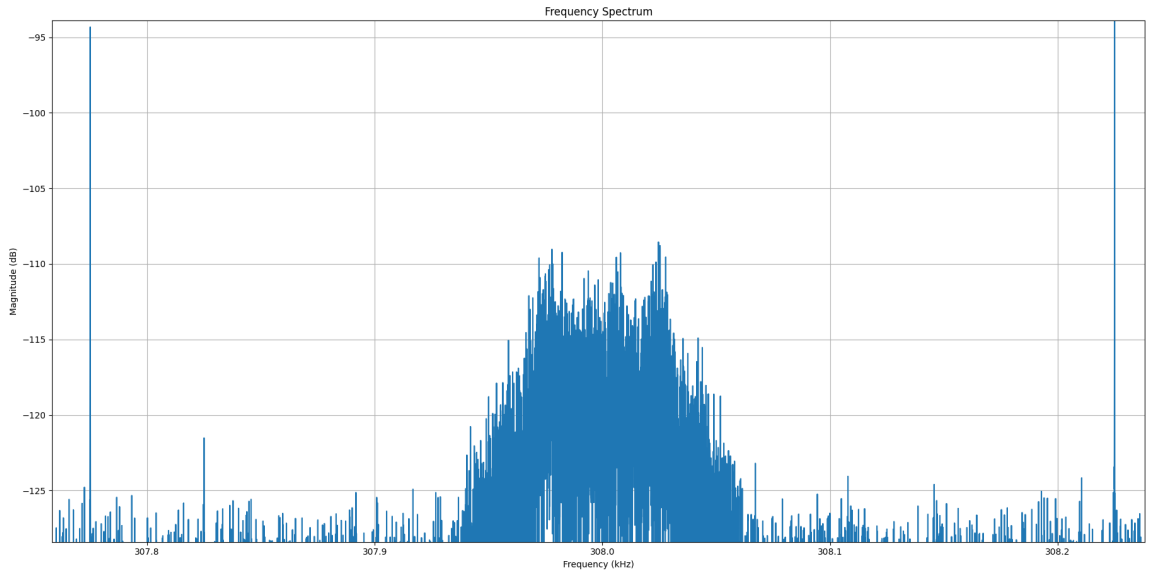

Figure 5.3: FFT of 1s of data, focusing on frequencies around 308 kHz (GrossMohdorf station) with peaks at sharply defined at 307 775Hz and 308 225 Hz

However, a convolution of a duration of 1s will only yield a resolution of 1 Hz (bins of size 1Hz), in other words, we do not have precision for frequency drifts below 1 Hz. ($\Delta f = \frac{1}{T_{obs}} = \frac{1}{1s} = 1Hz$)

One solution to increase the resolution is to increase the FFT time to 100s (to be precise down to the mHz), which is unfeasible. Performing FFT to recover frequency drifts that are lower than 1 Hz is therefore a method to be discarded.

5.3 System Robustness

From a practical standpoint, the GNU Radio implementation demonstrated high reliability, running continuously for several hours without de-synchronization or buffer underflow. Real-time decoding performance was achieved at moderate CPU utilization, confirming the computational efficiency of the pipeline. The frequency translating filter and symbol synchronizer blocks accounted for the majority of processing load, while the custom Python parity check and timestamp parser contribute negligibly.

Several operational limitations are to be noted. The 13-bit timestamp resolution (0.6 s) remains a fundamental restriction for absolute time recovery during cold start. Although the system maintained perfect relative synchronization once initialized, it could not independently derive the full UTC time without an external hint or prior synchronization event (Like a manual input). Furthermore, due to the non-deterministic nature of general-purpose operating systems, occasional timing offsets may be observed in scheduling-critical operations like that of the processing time calculation. These effects are expected to disappear with migration to a real-time operating system (RTOS) or dedicated SDR hardware with deterministic timing.

Another noteworthy observation concerns environmental susceptibility. While the rubidium oscillator provided excellent frequency stability during the recording of the data that was used to develop this thesis, small, long-term phase fluctuations are expected to be seen in the CW tones with regular quartz oscillator clocks.

Conclusion

This thesis has addressed the critical challenge of achieving resilient time synchronization in maritime navigation amid growing vulnerabilities in GNSS-dependent systems, such as jamming and spoofing observed in regions like the Baltic Sea. By leveraging the R-Mode framework, which repurposes existing medium-frequency maritime radio infrastructure, we have explored innovative methods for extracting precise time information from MSK-modulated signals and stabilizing local clock oscillators relative to remote atomic clock references.

Key contributions include a comprehensive analysis of time extraction techniques, demonstrating how the timestamp embedded in RTCM-formatted messages can be recovered through an SDR like GNU Radio, preamble detection, parity validation, and station ID verification. Simulations and theoretical derivations, including Cramer-Rao bounds for phase estimation under Gaussian noise, have quantified synchronization accuracy, revealing limitations in pure MSK-based positioning due to low bit rates and high timing uncertainties, while highlighting the advantages of incorporating CW signals for phase ranging and their impact on the final date-time solution. We have proposed and validated a novel approach to estimate processing delays using CW phase properties, achieving near-instantaneous corrections with minimal computational overhead. Furthermore, the implementation of a feedback loop for local oscillator stabilization, utilizing FFT-based frequency offset detection from the highest-SNR CW reference, ensures long-term clock stability, mitigating the inherent drift of quartz oscillators and maintaining synchronization during intervals between message broadcasts, such as the anticipated Message 55.

These advancements underscore the feasibility of R-Mode as a robust, GNSS-independent backup for timing, enhancing safety, coordination, and operational efficiency in maritime environments.

Future research could extend this by integrating real-time operating systems (RTOS) for deterministic processing, conducting field trials in diverse maritime conditions to validate the solution's accuracy. Ultimately, by reducing reliance on vulnerable satellite systems, this thesis advances the vision of autonomous, precise time recovery, aligning with international efforts to safeguard critical operations in an increasingly contested electromagnetic spectrum.

Bibliography

[1] ursanav, "ursanav.com," https://www.ursanav.com/wp-content/uploads/UrsaNav-ILA-40-eLoran-Signal-Specification-Tutorial.pdf, [Accessed 15-09-2025].

[2] M. Yang, B. Yan, C. Yang, X. Jiang, and S. Li, "Research on the eloran/gnss combined positioning algorithm and altitude optimization," *Remote Sensing*, vol. 17, no. 4, p. 633, 2025. [Online]. Available: https://doi.org/10.3390/rs17040633

[3] L. Grundhöfer, F. G. Rizzi, A. Damman, C. Rieck, M. Hoppe, M. Schütteler, and K. Bronk, "R-Mode Baltic 2 final report," R-Mode Baltic 2 Project / DLR (German Aerospace Center), Tech. Rep. Issue 1.0, October 2022, co-financed by the European Regional Development Fund within the Interreg Baltic Sea Region Programme. [Online]. Available: https://www.r-mode-baltic.eu/wp-content/uploads/2022/11/Final_report_R-Mode_Baltic2_v1.0.pdf

[4] "iala.int," https://www.iala.int/content/uploads/2016/08/accseas_r_mode_feasibility_study_mf_dgps_transmissions.pdf, [Accessed 10-10-2025].

[5] "World DGNSS Stations List - IALA — iala.int," https://www.iala.int/technical/positioning-navigation-and-timing/world-dgnss-stations-list/, [Accessed 20-09-2025].

[6] e. Redaktion dlr.de, as, "100 Years - Space flight in Germany &x2013; timeline including important events — web.archive.org," https://web.archive.org/web/20090624130230/http://www.dlr.de/100Jahre/en/desktopdefault.aspx/tabid-2581/4435_read-7391, [Accessed 21-10-2025].

[7] "About us — dlr.de," https://www.dlr.de/en/dlr/about-us, [Accessed 20-09-2025].

[8] "Institute of Communications and Navigation — dlr.de," https://www.dlr.de/en/kn, [Accessed 15-09-2025].

[9] "New optical ground station inaugurated at DLR's site in Oberpfaffenhofen — dlr.de," https://www.dlr.de/en/latest/news/2022/04/new-optical-ground-station-inaugurated-at-dlr-site-oberpfaffenhofen, [Accessed 15-09-2025].

[10] "Galileo Product Showcase - GPS World — gpsworld.com," https://www.gpsworld.com/galileo-product-showcase/, [Accessed 15-09-2025].

[11] D. Sobel, *Longitude: The True Story of a Lone Genius Who Solved the Greatest Scientific Problem of His Time*. London: Fourth Estate (UK), 1995.

[12] J. Trýb and J. Hospodka, "Gnss interference and security: Impacts on critical infrastructure and mitigation strategies," *Procedia Computer Science*, vol. 253, pp. 2635–2644, 2025, 6th

International Conference on Industry 4.0 and Smart Manufacturing. [Online]. Available: https://www.sciencedirect.com/science/article/pii/S187705092500331X

[13] J. M. Kolly, "Employing new technologies in marine accident investigations at the national transportation safety board," National Transportation Safety Board, Tech. Rep., 2010. [Online]. Available: https://www.nautinst.org/static/0c79c6ea-a289-4001-bffb6a42f179bd7a/HE00835-Employing-New-Technologies-in-Marine-Accident-Investigations-at-the-National-Transportation pdf

[14] G. Offermans, S. Bartlett, and C. Schue, "Providing a resilient timing and utc service using eloran in the united states," *NAVIGATION*, vol. 64, no. 3, pp. 339–349, 2017. [Online]. Available: https://onlinelibrary.wiley.com/doi/abs/10.1002/navi.197

[15] L. Grundhöfer, "R-mode: An alternative to global navigation satellite systems for terrestrial navigation at medium frequencies," Ph.D. dissertation, 07 2024.

[16] U.S. Department of Defense, "Global Positioning System Standard Positioning Service Performance Standard," U.S. Government Publishing Office, Tech. Rep. 5th Edition, July 2020, accessed: 09-20-2025. [Online]. Available: https://www.gps.gov/sites/default/files/2025-07/2020-SPS-performance-standard.pdf

[17] A. V. Oppenheim, R. W. Schafer, and J. R. Buck, "Discrete-time signal processing, 3pearson education," 2010.

[18] L. Grundhöfer, F. G. Rizzi, S. Gewies, M. Hoppe, J. Bäckstedt, M. Dziewicki, and G. Del Galdo, "Positioning with medium frequency r-mode," *NAVIGATION*, vol. 68, no. 4, pp. 829–841, 2021. [Online]. Available: https://elib.dlr.de/143889/1/NAVIGATION%20-%202021%20-%20Grundh%20fer%20-%20Positioning%20with%20medium%20frequency%20R%E2%80%90Mode.pdf

[19] "Skylake (client) - Microarchitectures - Intel - WikiChip — en.wikichip.org," https://en.wikichip.org/wiki/intel/microarchitectures/skylake_(client), [Accessed 17-09-2025].

[20] "G1187 Medium Frequency R-Mode signal structure and navigation message - IALA — iala.int," https://www.iala.int/product/g1187-medium-frequency-r-mode-signal-structure-and-navigation-message/, [Accessed 17-09-2025].

[21] piezoman.com, "Quartz resonators in the market," https://www.piezoman.com/product/1_Quartz.html, [Accessed 17-09-2025].